

mRNA vaccine-induced IgG mediates nasal SARS-CoV-2 clearance in mice

Charlie Fricke,¹ Lorenz Ulrich,² Jana Kochmann,¹ Janina Gergen,³ Kristina Kovacicova,³ Nicole Roth,³ Julius Beer,⁴ Daniel Schnepf,^{4,7} Thomas C. Mettenleiter,⁵ Susanne Rauch,³ Benjamin Petsch,^{3,8} Donata Hoffmann,² Martin Beer,² Björn Corleis,¹ and Anca Dorhoi^{1,6}

¹Institute of Immunology, Friedrich-Loeffler-Institut, 17493 Greifswald-Insel Riems, Germany; ²Institute of Diagnostic Virology, Friedrich-Loeffler-Institut, 17493 Greifswald-Insel Riems, Germany; ³CureVac SE, 72076 Tübingen, Germany; ⁴Institute of Virology, Medical Center University of Freiburg, 79104 Freiburg, Germany; ⁵Friedrich-Loeffler-Institut, 17493 Greifswald-Insel Riems, Germany; ⁶Faculty of Mathematics and Natural Sciences, University of Greifswald, 17489 Greifswald, Germany

Coronavirus disease 2019 (COVID-19) mRNA vaccines that have contributed to controlling the SARS-CoV-2 pandemic induce specific serum antibodies, which correlate with protection. However, the neutralizing capacity of antibodies for emerging SARS-CoV-2 variants is altered. Suboptimal antibody responses are observed in patients with humoral immunodeficiency diseases, ongoing B cell depletion therapy, and aging. Common experimental mouse models with altered B cell compartments, such as B cell depletion or deficiency, do not fully recapitulate scenarios of declining or suboptimal antibody levels as observed in humans. We report on SARS-CoV-2 immunity in a transgenic mouse model with restricted virus-specific antibodies. Vaccination of C57BL/6-Tg(IghelMD4)4Ccg/J mice with unmodified or N1mΨ-modified mRNA encoding for ancestral spike (S) protein and subsequent challenge with mouse-adapted SARS-CoV-2 provided insights into antibody-independent immunity and the impact of antibody titers on mucosal immunity. Protection against fatal disease was independent of seroconversion following mRNA vaccination, suggesting that virus-specific T cells can compensate for suboptimal antibody levels. In contrast, mRNA-induced IgG in the nasal conchae limited the local viral load and disease progression. Our results indicate that parenteral mRNA immunization can elicit nasal IgG antibodies that effectively suppress local viral replication, highlighting the potential of vaccines in controlling SARS-CoV-2 transmission and epidemiology.

INTRODUCTION

mRNA interventions are gaining importance, and comprehensive insights into mRNA-induced immunity are crucial. Antibodies induced by mRNA vaccination correlate with protection against COVID-19, yet their role in limiting viral transmission remains elusive.^{1,2} A role of T cells in vaccine-induced protection has been suggested by COVID-19 outcomes in patients with declining antibody titers or with humoral immunodeficiencies,^{3–7} and more recently by a mediation analysis for correlates of protection against newly emerging variants.⁸ Experimental models entirely lacking lymphocytes or antibodies inaccurately reflect the spectrum of human antibody levels.^{9,10} Here, we utilized C57BL/6-Tg(IghelMD4)4Ccg/J mice,

with few B cells expressing endogenous V genes,¹¹ to model host responses to mRNA immunization in individuals with limited capabilities to produce virus-specific antibodies.^{12,13} In IghelMD4 mice, 95% of splenic B cells carry the IghelMD4 transgene that recognizes hen egg lysozyme.¹¹ The spleen architecture and frequencies of CD4⁺ T cells are unchanged, whereas CD8⁺ T and B cells are fewer than in wild-type (WT) littermates. In this model, subunit vaccines trigger effective cellular immune responses with partially reduced CD8 immunity,¹⁴ while limited levels of pathogen-specific antibodies are elicited upon immunization.^{12,13}

Here, we challenged these animals with the mouse-adapted strain SARS-CoV-2 MA20,^{15,16} included males and females, and vaccinated with mRNA to evaluate the impact of sex and vaccine features on immunogenicity and protection against SARS-CoV-2. We previously described T cell responses in mice vaccinated with unmodified mRNA.¹⁷ For comparison, we used unmodified (male-only) mRNA alongside N1mΨ-modified mRNA, widely applied in humans. The study demonstrates the ability of T cells to protect against lethal disease by indicating that virus-specific antibodies are redundant for survival in mice. Antibody titers correlated with viral clearance in nasal tissue and limited disease severity. mRNA vaccination induced nasal anti-spike IgG antibodies necessary for local clearance of SARS-CoV-2.

RESULTS

mRNA-vaccinated WT and IghelMD4 mice develop comparable virus-specific T cell responses

To investigate the role of T cells in the context of limited antibody production, we vaccinated male and female IghelMD4 or WT

Received 28 June 2024; accepted 10 October 2024;
<https://doi.org/10.1016/j.omtn.2024.102360>.

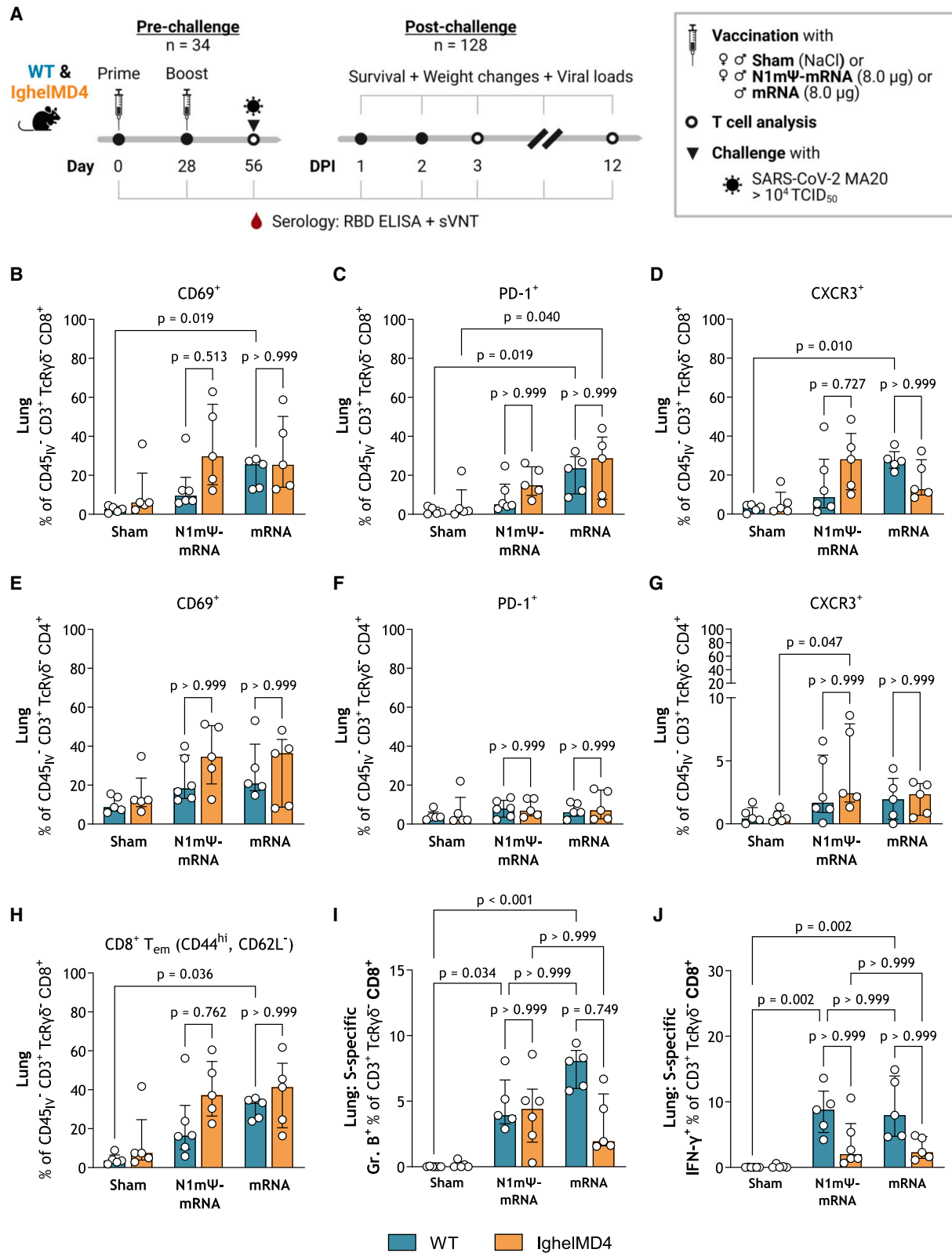
⁷Present address: The Francis Crick Institute, London NW1 1AT, UK

⁸Present address: Cipla Europe NV, 82008 Unterhaching, Germany

Correspondence: Björn Corleis, Institute of Immunology, Friedrich-Loeffler-Institut, 17493 Greifswald-Insel Riems, Germany.
E-mail: bjoern.corleis@fli.de

Correspondence: Anca Dorhoi, Institute of Immunology, Friedrich-Loeffler-Institut, 17493 Greifswald-Insel Riems, Germany.
E-mail: anca.dorhoi@fli.de





(legend on next page)

littermate controls twice with modified N1m Ψ -mRNA or unmodified mRNA encoding for the spike (S) protein of ancestral SARS-CoV-2. Subsequently, we challenged them with a mouse-adapted SARS-CoV-2 (Figure 1A; Table S1), which causes pulmonary disease and viral replication in the upper respiratory tract.¹⁶ We first evaluated tissue-residing T cells upon immunization using intravenous delivery of a CD45 antibody (Figure S1A).¹⁸ Vaccine-induced CD45^{IV}[−] T cell responses were more pronounced for CD8⁺ than CD4⁺ T cells (Figures 1B–1H, S1B–S1G, and S2) as described previously.¹⁷ Activation and homing of CD45^{IV}[−] CD8⁺ T cells from mice of both genotypes were primarily detectable in the lung compared with spleen after mRNA vaccination, as demonstrated by the increased expression of CD69, PD-1, and CXCR3 (Figures 1B–1G and S1B–S1G). We observed an increase in CD8⁺ T effector memory cells (T_{em}: CD45^{IV}[−], CD44^{hi}, CD62L[−]) while total T cell numbers in the lungs and spleen remained similar to those observed in Sham-vaccinated animals (Figures 1H and S2). S peptide-specific T cell responses were measured by evaluating IFN- γ and granzyme B (Figure S3A). Robust SARS-CoV-2-specific T cell responses were detectable in both mouse strains without significant differences between the genotypes and vaccine constructs (Figures 1I, 1J, and S3B–S3E). No sex differences in T cell populations were observed (Figure S2). Thus, T cell responses appeared similar between WT and IghelMD4 mice after mRNA vaccination.

mRNA-vaccinated WT and IghelMD4 mice show distinct levels of neutralizing antibodies

We evaluated vaccine-induced humoral responses by assessing seroconversion over time. All WT mRNA-vaccinated mice elicited high anti-RBD serum antibodies (Figures 2A–2C) with high neutralizing capacity (Figures 2D–2F) as early as d28 (pre-boost). Fifteen out of 34 N1m Ψ -mRNA- and 5/15 mRNA-vaccinated IghelMD4 mice seroconverted by day 56 (Figures 2D–2F). Most vaccinated IghelMD4 mice developed significantly lower antibody levels (Figures 2B and 2C) and neutralizing capacity (Figures 2D–2F) than WT counterparts. Based on the SARS-CoV-2 antibody spectrum, we divided the IghelMD4 mice into seroconverters and non-seroconverters to better understand the role of humoral immunity in disease protection. The abundance of RBD-specific antibodies correlated with neutralization titers ($r_s = 0.883$, $p = 7.318 \times 10^{-55}$), demonstrating that high antibody titers reflect neutralizing capacity in this model (Figure S4A). Thus, WT and IghelMD4 mice elicited significantly different levels of neutralizing serum antibodies, irrespective of the

type of mRNA vaccine (Figures 2B and 2C) and the sex of the animals (Figure S4B).

Virus-specific serum antibodies define disease progression without affecting survival

We performed an initial experiment to determine whether IghelMD4 mice have a similar dose-dependent susceptibility to SARS-CoV-2 MA20 as WT mice (Figures S5A and S5C). Application of $10^{4.45}$ TCID₅₀ led to a 50%–70% survival rate and a similar course of infection in mice of both genotypes (Figures S5B and S5C). Of note, only 1/13 IghelMD4 but 9/9 unvaccinated WT mice seroconverted (Figure S5D) by 10 DPI, reflecting the restricted B cell receptor repertoire of IghelMD4 mice.¹¹ Next, we investigated the susceptibility of vaccinated IghelMD4 mice to SARS-CoV-2 MA20 challenge. Both mRNA vaccines effectively protected all mice from lethal diseases (Figure 3A). The vaccine-conferred protection was independent of seroconversion (Figure 3B) and sex (Figures S6A and S6B). We determined disease progression by monitoring individual changes in body weight (Figure S7). In contrast to unvaccinated WT mice, IghelMD4 mice exhibited delayed weight recovery, and mRNA-vaccinated IghelMD4 mice showed a detectable but insignificant early weight loss (Figure 3C). For both N1m Ψ -mRNA- and mRNA-vaccinated IghelMD4 mice, only seronegative (d56) mice showed a significant weight loss within the first 6 DPI (Figure 3D), with no sex differences (Figures S6C and S6D). This suggests that virus-specific antibodies induced by mRNA vaccination can prevent disease progression, such as weight loss, but are not necessary to prevent lethal outcomes.

Antibody and T cell responses differ between mRNA-vaccinated WT and IghelMD4 mice upon SARS-CoV-2 infection

To evaluate the impact of T cell responses on disease fatality, T cell responses in the lung (Figures 4A–4C, S8A–S8C, and S9A–S9F) and spleen (Figures 4D–4F, S8D–S8F, and S9G–S9L) in IghelMD4 mice with low serum anti-SARS-CoV-2 antibodies and WT mice were monitored after viral challenge. CD8⁺ T_{em} cell frequencies of both genotypes were similarly elevated at 12 DPI, mainly in vaccinated mice and predominantly in the spleen (Figures S9F and S9L). WT and IghelMD4 mice elicited comparable S-specific IFN- γ and granzyme B production by lung and spleen T cells (Figures S10A–S10F). The abundance of S peptide-specific IFN- γ -producing lung CD8⁺ T cells did not correlate ($r_s = 0.076$, $p = 0.6901$) with weight at 12 DPI in IghelMD4 mice (Figure S10G). Regardless of vaccination status, IghelMD4 mice had elevated frequencies of activated lung

Figure 1. WT and IghelMD4 mice exhibit similar SARS-CoV-2-specific T cell responses

(A) Study design: female (♀) and male (♂) WT and IghelMD4 mice ($n = 162$) were primed (day 0) and boosted (day 28) with NaCl (Sham), 8.0 μ g N1m Ψ -mRNA, or 8.0 μ g unmodified mRNA vaccines encoding the S protein of SARS-CoV-2. On day 56, 128 mice ($n = 128$) were challenged with $>10^4$ TCID₅₀ of SARS-CoV-2 MA20 in three independent experiments. Mice were analyzed for anti-SARS-CoV-2 antibodies in nasal tissue and serum and T cell responses in the lungs and spleen before and after the challenge. Survival, weight changes, and viral loads were monitored up to 12 DPI or upon reaching the humane endpoint criteria. Created with BioRender.com. (B–H) Tissue-residing (CD45^{IV}[−]) T cells from the lungs of mice were analyzed for CD69 (B and E), PD-1 (C and F), CXCR3 (D and G) expression, and frequencies of CD8⁺ effector memory T cells (H). (I and J) Single-cell suspensions obtained from the lungs of mice were restimulated *in vitro* with S peptides. The percentage of CD8⁺ T cells that expressed granzyme B (I) or IFN- γ (J) in the lungs (day 56) is depicted. The values were obtained by subtracting percentage (unstimulated) from percentage (S peptide stimulated). (B–J) Each data point represents one animal. $n = 5$ per vaccine and mouse group. $n = 6$ for Sham WT and N1m Ψ -mRNA IghelMD4. The median with the interquartile range is displayed. p values were determined by nonparametric one-way ANOVA and Dunn's multiple comparison test.

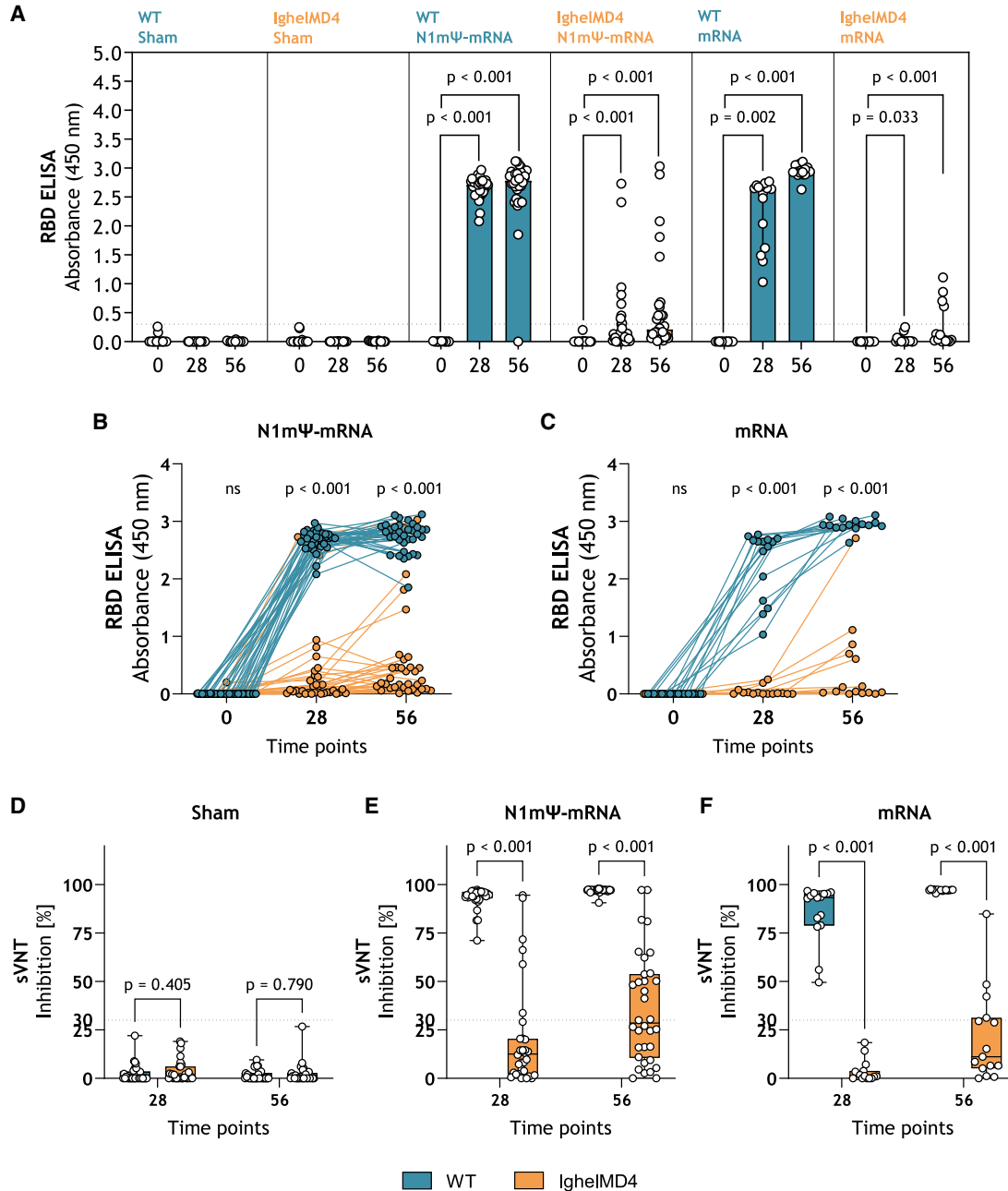


Figure 2. WT and IgheIMD4 mice elicit distinct levels of neutralizing antibodies upon mRNA vaccination

(A) RBD ELISA of serum from Sham- or mRNA-vaccinated mice pre-challenge. Number of animals per time point: $n = 33$ for Sham WT, $n = 30$ for Sham IgheIMD4, $n = 35$ for N1mΨ-mRNA WT, $n = 34$ for N1mΨ-mRNA IgheIMD4, $n = 15$ for mRNA WT and IgheIMD4. The dotted line (...) represents the cutoff for seroconversion (OD = 0.3). The median with the interquartile range is displayed. p values were determined by nonparametric one-way ANOVA and Dunn's multiple comparison test. (B and C) Statistical analysis of matched RBD ELISA samples. Number of animals per time point: $n = 35$ for N1mΨ-mRNA WT, $n = 34$ for N1mΨ-mRNA IgheIMD4, $n = 15$ for mRNA WT and IgheIMD4. p values were determined by two-way ANOVA and Šidák's multiple comparisons test. (D–F) Surrogate virus neutralization test (sVNT) at days 28 and 56 for Sham (D), N1mΨ-mRNA (E), and unmodified mRNA (F). Number of animals per time point: $n = 34$ for Sham WT, $n = 30$ for Sham IgheIMD4, $n = 35$ for N1mΨ-mRNA WT, $n = 34$ for N1mΨ-mRNA IgheIMD4, $n = 15$ for mRNA WT and IgheIMD4. Error bars represent the min to max range. p values were determined by two-way ANOVA with Šidák's multiple comparisons test. The dotted line (...) represents the cutoff for sVNT positivity (30% inhibition) according to the manufacturer's manual. (A–F) Each data point represents one animal.

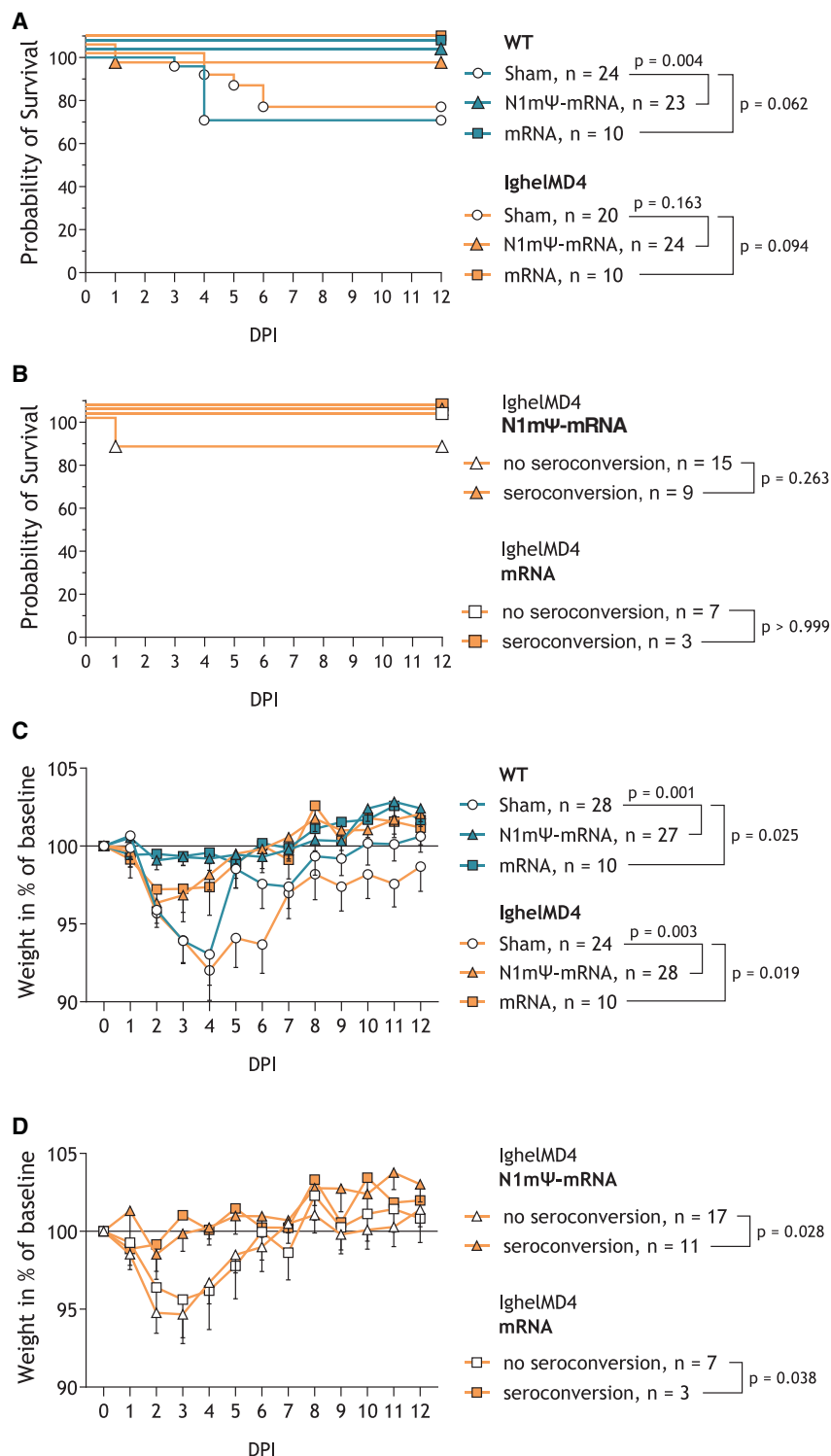


Figure 3. mRNA vaccine-induced serum antibody levels determine disease progression without impacting survival

(A and B) Survival analysis for Sham, N1mΨ-mRNA, or mRNA vaccinated WT and IgheIMD4 mice (A) and IgheIMD4 mice vaccinated with N1mΨ-mRNA or mRNA divided by seroconversion status (B) after infection with SARS-CoV-2 MA20 up to 12 DPI. p values were determined by direct curve comparison (Kaplan-Meier) using log rank (Mantel-Cox) test. (A) Number of animals: $n = 24$ for Sham WT, $n = 20$ for Sham IgheIMD4, $n = 23$ for N1mΨ-mRNA WT, $n = 24$ for N1mΨ-mRNA IgheIMD4, $n = 10$ for mRNA WT and IgheIMD4. (B) Number of animals: $n = 15$ for N1mΨ-mRNA no seroconversion, $n = 9$ for N1mΨ-mRNA seroconversion, $n = 7$ for mRNA no seroconversion, $n = 3$ for mRNA seroconversion. (C and D) Weight changes of mice infected with SARS-CoV-2 MA20 until 12 DPI for Sham, N1mΨ-mRNA, or mRNA vaccinated WT and IgheIMD4 mice (C) and IgheIMD4 mice vaccinated with N1mΨ-mRNA or mRNA divided by seroconversion status (D). The dataset passed the D'Agostino-Pearson normality test ($\alpha = 0.05$). Each data point represents the mean with SEM. p values were determined by two-way ANOVA (mixed effects analysis). (C) Number of animals: $n = 28$ for Sham WT, $n = 24$ for Sham IgheIMD4, $n = 27$ for N1mΨ-mRNA WT, $n = 28$ for N1mΨ-mRNA IgheIMD4, $n = 10$ for mRNA WT and IgheIMD4. (D) Number of animals: $n = 17$ for N1mΨ-mRNA no seroconversion, $n = 11$ for N1mΨ-mRNA seroconversion, $n = 7$ for mRNA no seroconversion, $n = 3$ for mRNA seroconversion. (A–D) Exclusion of animals that reached the predetermined study endpoint at 3 DPI ($n = 4$ per group for Sham and N1mΨ-mRNA) from survival analysis caused differences in the number of animals in survival (A and B) and weight change plots (C and D) for each group.

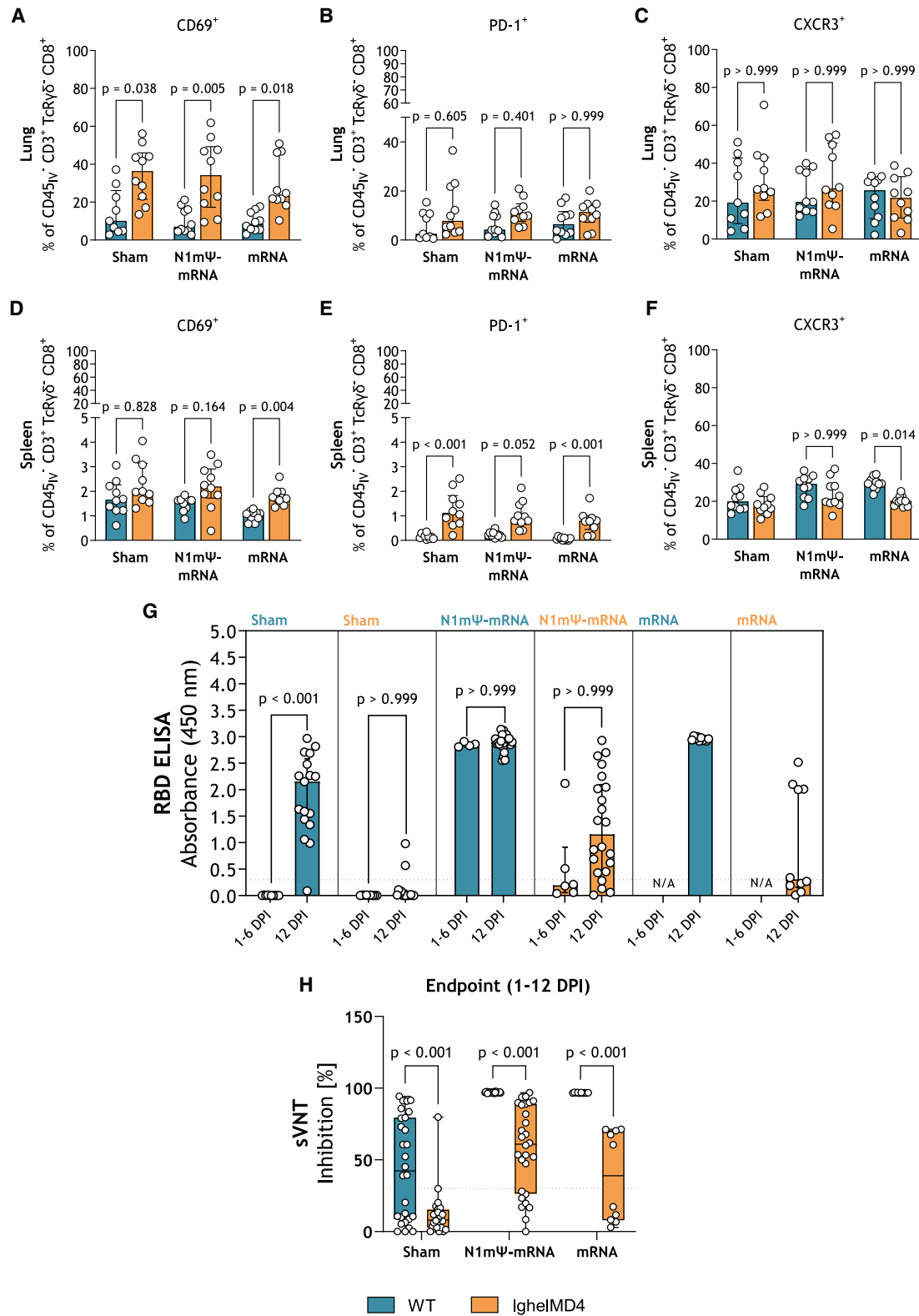
of serum anti-RBD antibodies post-challenge, which increased by 12 DPI in IgheIMD4 mice compared with pre-challenge (Figure 4G). However, neutralization capacity was significantly reduced compared with WT mice (Figure 4H). Thus, increased T cell activation upon infection in IgheIMD4 mice with limited antibody levels may contribute to the prevention of fatal outcomes.

mRNA-induced mucosal IgGs confer nasal clearance of SARS-CoV-2

Next, we investigated viral loads in WT and IgheIMD4 mice. Viral RNA was not detected in the lungs of vaccinated WT mice at 1–6 DPI, whereas it was present in IgheIMD4 mice and Sham-vaccinated controls (Figure S11A). After

CD69⁺CD8⁺ and spleen PD-1⁺CD8⁺ T cells post-infection, whereas frequencies of CXCR3 expressing cells remained similar to WT littermates (Figures 4A–4F and S8A–S8F). We monitored the abundance

12 DPI, almost all surviving mice cleared the virus from the lungs, regardless of genotype and immunization status (Figure S11B). In the conchae, early post-challenge, vaccinated WT mice and



(legend on next page)

IghelMD4 mice showed significantly lower viral RNA levels than Sham-vaccinated control groups (Figure S11C). Later, vaccination with N1mΨ-mRNA or unmodified mRNA restricted nasal viral loads in WT, but not in IghelMD4 mice (Figure 5A), irrespective of the sex (Figures S11D and S11E). Serum anti-RBD antibodies from all groups and genotypes negatively correlated ($r_s = -0.751$, $p = 3.98 \times 10^{-24}$) with viral RNA loads in the conchae (Figures 5A and 5B). In Sham-vaccinated animals, viral loads in the conchae correlated with disease severity at 12 DPI (Figure 5C). A weak negative correlation ($r_s = -0.507$, $p = 0.0042$) of S peptide-specific CD8⁺ IFN- γ ⁺ lung T cells with viral loads in conchae was observed (Figure 5D). Since anti-RBD antibodies correlated with viral clearance in the nasal conchae, we monitored local S-specific IgG1 and IgG2c in vaccinated mice in this compartment. Despite elevated levels of anti-RBD serum antibodies, SARS-CoV-2 infection alone did not induce local IgG responses within 12 DPI (see Sham animals in Figures 5E–5H). Vaccination with either N1mΨ-mRNA (Figures 5E–5H) or unmodified mRNA (Figures 5G and 5H) induced IgG1 and IgG2c in the conchae of WT mice but not in IghelMD4 mice during the first week (Figures 5E and 5F) and by 12 DPI (Figures 5G and 5H). Although several IghelMD4 mice developed anti-RBD and neutralizing antibodies in the serum during infection (Figures 4G and 4H), these could not limit nasal viral RNA load in the absence of local IgG. Only mice with detectable IgG in the conchae cleared the virus from this compartment (Figures 5A–5H). Thus, mRNA vaccination contributes to mucosal clearance of SARS-CoV-2 by induction of nasal IgGs.

DISCUSSION

Insights into immunity in individuals with impaired humoral responses upon mRNA vaccination are limited, and current models fail to reflect the broad spectrum of antibody levels in the human population. Using the IghelMD4 mouse model, we, in line with others, found that mRNA vaccination-induced virus-specific T cell responses can compensate for limited antibody titers to protect against a lethal SARS-CoV-2 challenge.^{9,19,20} Viral loads were only detected in the lungs of Sham-vaccinated mice and IghelMD4 mice early after infection, strongly suggesting that immunization can induce virus-specific antibodies that effectively prevent the virus from spreading to the lower respiratory tract. The correlation of disease severity and negative correlation of serum anti-RBD antibodies with conchae viral loads supports a critical role of virus-specific antibodies in viral clearance from the nose and disease progression, consistent with previous studies.²¹ T cells are likely to have a minor contribution to SARS-

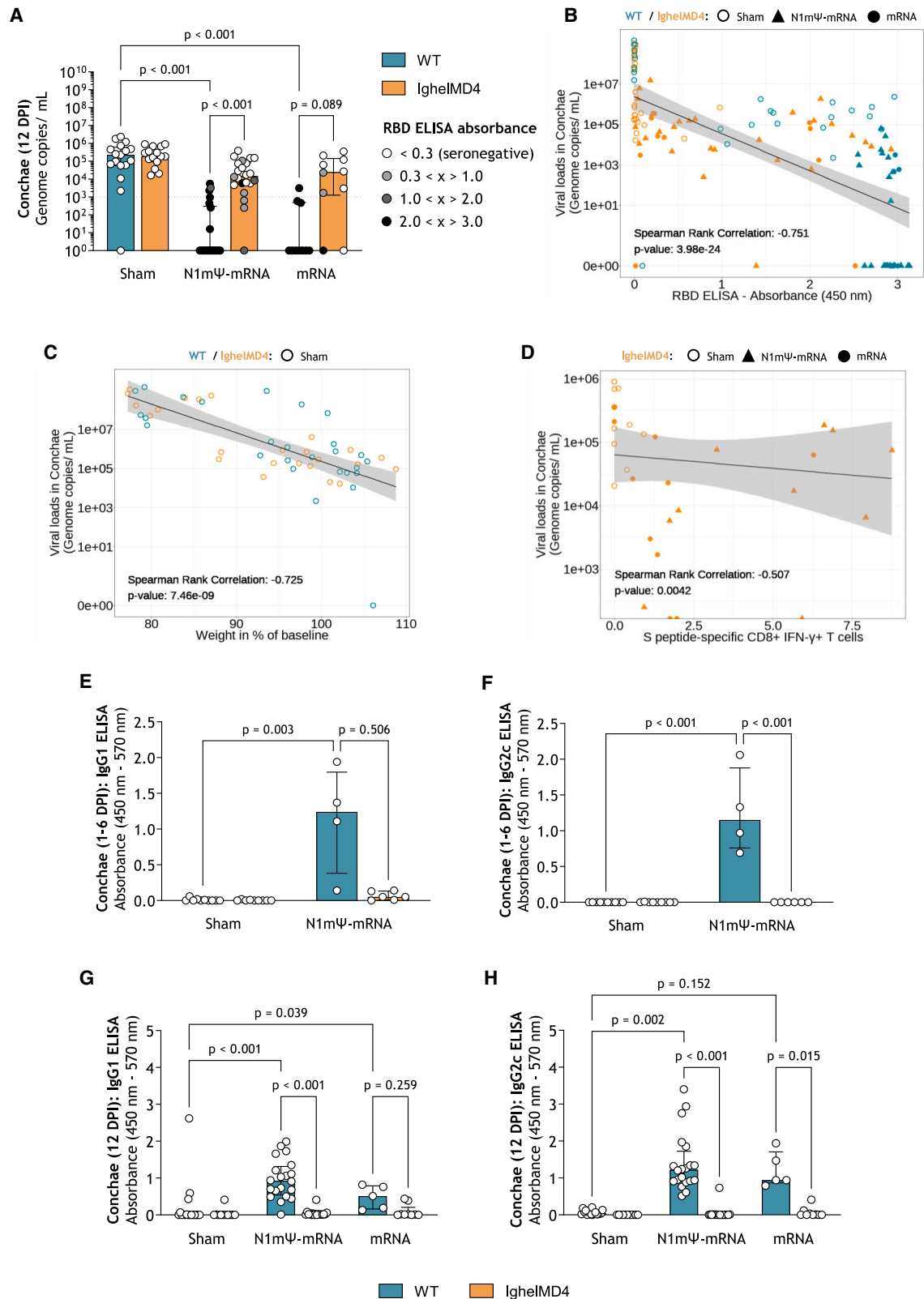
CoV-2 nasal clearance after mRNA vaccination since only a weak negative correlation of virus-specific lung T cells with viral loads in conchae was observed. However, we did not measure T cell responses in the nasal compartment and cannot exclude a possible contribution to mucosal viral clearance, as recently reported.^{8,22,23} SARS-CoV-2-specific CD4⁺ and CD8⁺ tissue-resident memory T cells (T_{rm}) have been identified in the human upper airways.²⁴ Our results suggest that parenterally delivered mRNA vaccines may help to develop mucosal immunity against SARS-CoV-2 in the nose by inducing local IgGs. These results are consistent with recently published studies reporting the induction of mucosal IgGs following mRNA vaccination in humans,^{25–32} which may contribute to the inhibition of human-to-human transmission.^{27,28} However, as nasal antibody measurements were performed post-challenge, we cannot conclude on the stimulation of mucosal IgG by mRNA vaccination alone. Further, the potential of the IghelMD4 mice to clear the virus in the conchae beyond 12 DPI remains unknown.

We did not observe statistically significant differences in T cell responses between WT and IghelMD4 mice after vaccination. However, there may be variability in T cell responses after infection, which has also been observed in the IghelMD4 model by others.¹⁴ The variations in T cell activation between WT and IghelMD4 mice following infection suggest a potential role in protecting against fatal disease in animals with limited antibody responses. This protection may develop independently from vaccine-induced protection mediated by antibodies, as similar differences were present in Sham-vaccinated WT and IghelMD4 mice. Depleting T cells in mice with restricted antibody levels would confirm their role in protecting against SARS-CoV-2 lethality. We did not measure T cells in nasal conchae, and depletion of tissue-residing T cells may be cumbersome in this compartment. Total ablation of mucosal residing subsets would permit concluding on their roles during infection. Finally, we did not compare mRNA vaccines with other vaccine platforms, such as viral vector vaccines and routes of administration (e.g., intranasal), to explore the effectiveness of triggering mucosal antibodies for SARS-CoV-2 clearance. Yet, our experimental animal model data support the mucosal benefits of parenteral mRNA vaccines.

Using a mouse model with a reduced ability to mount antigen-specific antibody responses after immunization, we found that immunity mediated by virus-specific antibodies can limit disease progression. Virus clearance in the nasal mucosa was only achieved with mucosal

Figure 4. WT and IghelMD4 mice display distinguishing antibody and T cell responses following SARS-CoV-2 MA20 infection

(A–F) Tissue-residing (CD45_{low}) T cells from the lungs (A–C) and spleen (D–F) of mice were analyzed at 12 DPI for CD69 (A and D), PD-1 (B and E), and CXCR3 (C and F) expression. Number of animals: $n = 10$ per vaccine and mouse group, $n = 9$ for Sham WT (lungs). The median with the interquartile range is displayed. (G) Analysis of RBD ELISA of serum samples from Sham-, N1mΨ-mRNA-, or mRNA-vaccinated mice at 1–6 and 12 DPI. Number of animals: $n = 10$ (1–6 DPI) and $n = 17$ (12 DPI) for Sham WT, $n = 9$ (1–6 DPI) and $n = 15$ (12 DPI) for Sham IghelMD4, $n = 4$ (1–6 DPI) and $n = 23$ (12 DPI) for N1mΨ-mRNA WT, $n = 6$ (1–6 DPI), and $n = 22$ (12 DPI) for N1mΨ-mRNA IghelMD4, $n = 10$ (12 DPI) for mRNA WT and IghelMD4. The dotted line (...) represents the cutoff for seroconversion (OD = 0.3). (A–G) p values were determined by nonparametric one-way ANOVA and Dunn's multiple comparison test. (H) Surrogate virus-neutralization test (sVNT) at 1–12 DPI for Sham-, N1mΨ-mRNA-, or mRNA-vaccinated WT and IghelMD4 mice. Number of animals: $n = 28$ for Sham WT, $n = 27$ for Sham IghelMD4, $n = 27$ for N1mΨ-mRNA WT, $n = 28$ for N1mΨ-mRNA IghelMD4, $n = 10$ for mRNA WT and IghelMD4. Error bars represent the min to max range. p values were determined by two-way ANOVA with Sidák's multiple comparisons test. The dotted line (...) represents the cutoff for sVNT positivity (30% inhibition). (A–H) Each data point represents one animal.



(legend on next page)

spike-specific IgG antibody responses, indicating the importance of local immunity in limiting virus replication. Induction of mucosal IgG after infection was abundant in mRNA-vaccinated animals, supporting a critical role for mRNA vaccines in limiting virus transmissibility. These mucosal effects triggered by mRNA vaccination may provide benefits beyond SARS-CoV-2 vaccination.

MATERIALS AND METHODS

Ethics, biosafety, and virus preparation

The animal experiments were evaluated and approved by the ethics committee of the State Office of Agriculture, Food safety, and Fishery in Mecklenburg-Western Pomerania (LALLF M-V: 7221.3-1-055/20). All procedures using SARS-CoV-2 were carried out in approved biosafety level 3 facilities. Virus stocks were generated as described previously.¹⁶ SARS-CoV-2 MA20 stocks were produced by one-time passaging using Vero E6 cells.

Animal housing

WT littermates (C57BL/6) and IghelMD4 transgenic (C57BL/6-Tg(IghelMD4)4Ccg/J) female and male mice were purchased from Charles River Laboratories (Sulzfeld, Germany) at age 6–8 weeks, kept in groups of up to five animals and provided with unlimited access to water and food. Infected mice were housed in individually ventilated cages upon challenge. Animals were housed at 20°C–24°C temperature, 45%–65% humidity, and 12 h dark/light cycle with 30 min of dawn.

Immunization

Mice ($n = 162$) received 20 μL of either 8.0 μg modified CV2CoV, unmodified CV2CoV, or 0.9% NaCl (Sham) intramuscularly into *M. tibialis* using a BD Micro-Fine 0.5 mL insulin syringe with a 30 G \times 8 mm needle. Vaccination was performed in four individual experiments. Both vaccines encoded for the SARS-CoV-2 S protein (NCBI reference sequence: NC_045512.2, GenBank accession number: YP_009724390.1), including K986P and V987P mutations. Vaccines were delivered in lipid nanoparticles from Acuitas Therapeutics (Vancouver, Canada), consisting of ionizable aminolipid, phospholipid, cholesterol, and a PEGylated lipid. Modified CV2CoV (N1m Ψ -mRNA) contained N1-methylpseudouridine (N1m Ψ) modified mRNA, while unmodified CV2CoV (mRNA) did not include chemically modified nucleosides as described previ-

ously.^{17,33,34} A total of 34 mice were used to analyze pre-challenge immune responses.

Challenge infection

Mice ($n = 127$) were challenged in three independent experiments intranasally under short-term isoflurane inhalation anesthesia with $10^{4.46}$, $10^{4.27}$, and $10^{4.46}$ TCID₅₀ SARS-CoV-2 MA20. In a prior dose-finding experiment, mice were infected with $10^{2.62}$ ($n = 12$) or $10^{4.45}$ TCID₅₀ ($n = 15$) SARS-CoV-2 MA20. Body weight and clinical score were monitored daily. Animals reaching the human endpoint criteria were euthanized. Few animals receiving NaCl (Sham) or N1m Ψ -mRNA ($n = 4$ for each mouse genotype) reached a predetermined study endpoint at 3 DPI and were consequently excluded from survival analysis. One WT mouse vaccinated with N1m Ψ -mRNA suffered an infection-unrelated death during challenge infection due to anesthesia procedures and was excluded from the analysis. All remaining mice were euthanized at 12 DPI.

Sampling and tissue processing

Blood was collected into Z-clot activator microtubes (Sarstedt, Nümbrecht, Germany) and sera were stored at -20°C . For sera inactivation, lung, spleen, and conchae were harvested as described previously.³⁵

Cell isolation and flow cytometry

Cells from lung and spleen tissue were isolated and stained for flow cytometry as described previously.^{17,35} Specific monoclonal antibodies were used to identify different types of immune cell subsets (Table S2). Samples were acquired using the BD LSR Fortessa Cell Analyzer from Becton Dickinson (Franklin Lakes, NJ). Data were analyzed using BD FACSDiva and FlowJo (version 10.5.3).

In vitro restimulation

Cells were restimulated *in vitro* with SARS-CoV-2 spike peptides, and lymphocyte cytokine release was measured using flow cytometry as described previously.³⁵

Detection of RBD-specific antibody levels

Anti-RBD (ancestral SARS-CoV-2) antibodies were detected using the previously described protocol for enzyme-linked immunoassay assay.³⁶

Figure 5. Mucosal IgG is required to clear SARS-CoV-2 from the conchae of experimentally infected mice

(A) Viral loads in the conchae of SARS-CoV-2 MA20-infected mice on 12 DPI. The detection limit was set at 10^3 viral RNA copies per mL, represented by a dotted line (...). Number of animals: $n = 17$ for Sham WT, $n = 15$ for Sham IghelMD4, $n = 23$ for N1m Ψ -mRNA WT, $n = 22$ for N1m Ψ -mRNA IghelMD4, $n = 10$ for mRNA WT and IghelMD4. (B–D) Linear regression and correlation analysis of conchae viral loads with RBD ELISA absorbance (day of death) (B), weight on the day of death for Sham-vaccinated animals (C), and S peptide-specific CD8⁺ IFN- γ ⁺ T cells for IghelMD4 mice at 12 DPI (D). (E–H) IgG1 (E and G) and IgG2c (F and H) ELISA of conchae homogenized tissue supernatants on 1–6 (E and F) and 12 DPI (G and H). (E and F) Number of animals: $n = 10$ for Sham WT, $n = 9$ for Sham IghelMD4, $n = 4$ for N1m Ψ -mRNA WT, $n = 6$ for N1m Ψ -mRNA IghelMD4. (G and H) Number of animals: $n = 17$ for Sham WT, $n = 11$ for Sham IghelMD4, $n = 20$ for N1m Ψ -mRNA WT, $n = 17$ for N1m Ψ -mRNA IghelMD4, $n = 5$ for mRNA WT, $n = 9$ for mRNA IghelMD4. (A and E–H) Each data point represents one animal. The median with the interquartile range is displayed. p values were determined by nonparametric one-way ANOVA and Dunn's multiple comparison test. (B) Number of animals: $n = 27$ for Sham WT, $n = 24$ for Sham IghelMD4, $n = 27$ for N1m Ψ -mRNA WT, $n = 28$ for N1m Ψ -mRNA IghelMD4, $n = 10$ for mRNA WT and IghelMD4. (C) Number of animals: $n = 27$ for WT, $n = 24$ for IghelMD4. (D) Number of animals: $n = 10$ per condition. (B–D) Two-tailed Spearman rank correlation was performed with R (version 4.3.2) in R studio (2023.12.1 build 402) using cor.test(). The regression line was added using geom_smooth() and the linear model (lm) method within the ggplot2 visualization package. The gray area represents the 95% confidence interval.

Surrogate virus neutralization test

The surrogate virus neutralization test (sVNT) was performed using the cPass SARS-CoV-2 Neutralization Antibody Detection Kit from GeneScript Biotech (Nanjing City, China) following the manufacturer's instructions. Absorbance was measured using the Tecan Infinite 200 Pro (Tecan Group AG, Männedorf, Switzerland).

RNA extraction for RT-qPCR

Sample processing was performed using established protocols.³³ RNA from organ samples was extracted using the NucleoMag VET Kit (Macherey-Nagel, Düren, Germany) and the Biosprint 96 platform (QIAGEN, Hilden, Germany). Real-time RT-qPCR quantified viral RNA with the CFX96 detection system (Bio-Rad Laboratories, Hercules) targeting the viral RNA-dependent RNA polymerase.

Detection of spike-specific IgG1 and IgG2c antibodies

Nunc MaxiSorp ELISA plates (BioLegend, Koblenz, Germany) were coated with 1.5 µg/mL SARS-CoV-2 spike protein (S1+S2) ECD His tag (cat. no. 40589-V08B1; Sino Biological Europe, Düsseldorf, Germany) in PBS overnight at 4°C. After washing with wash buffer (0.05% Tween 20 in PBS), plates were blocked for 3 h 30 min at room temperature (RT) with blocking buffer (5% skim milk powder in PBS). Samples were diluted at 1:80 for IgG1 and 1:10 for IgG2c ELISA in a serum-free medium. Fifty microliters was added into the wells and incubated for 2 h at RT. After washing, 50 µL of Biotin anti-mouse IgG1 (BioLegend; cat. no. 406603) or IgG2a/c (BioLegend; cat. no. 407103) antibodies diluted 1:300 in blocking buffer were added and incubated for 1 h at RT. Following washing, wells were incubated for 30 min at RT with NeutrAvidin-HRP (Thermo Fisher Scientific, Waltham, MA; 1:10,000 in 1× PBS/0.05% Tween 20), followed by another washing step. Fifty microliters of 1-step-Ultra-TMB-ELISA substrate (Thermo Fisher Scientific) was added and incubated for 5 min at RT before stopping with 50 µL 20% H₂SO₄. Absorbance was measured at 450 and 570 nm (reference wavelength) using Tecan Infinite 200 Pro (Tecan Group, Männedorf, Switzerland). Antibody levels were normalized by total protein abundance in samples, which was determined with the Pierce BCA Protein Assay Kit (Thermo Fisher Scientific) following the manufacturer's protocol.

Statistical analysis

Calculations were performed using GraphPad prism version 10.2.0 (GraphPad Software, San Diego, CA) for Windows. Two-tailed Spearman correlation analysis was performed with R (version 4.3.2) in R studio (2023.12.1 build 402) using cor.test(). Details are provided within the figure legends. Data were tested for normal distribution using the D'Agostino-Pearson normality test ($\alpha = 0.05$). Results with *p* values less than 0.05 were considered significant.

DATA AND CODE AVAILABILITY

The data supporting this study's findings are available from the corresponding author upon reasonable request.

ACKNOWLEDGMENTS

The authors thank Laura Timm, Gabriele Stooß, Ulrike Zedler, and Mareen Grawe for their excellent technical assistance. We thank Frank Klipp, Doreen Fiedler, Christian Lipinski, Steffen Kiepert, Bärbel Berger, and Kerstin Kerstel for their support in the animal facility. This research was supported by funds from BMBF (01KI20703), CureVac SE, and GSK.

AUTHOR CONTRIBUTIONS

C.F. designed, performed, and analyzed the experiments, and wrote the paper. J.K. and L.U. performed specific experiments and reviewed the paper. J.G., K.K., N.R., S.R., and B.P. provided advice and reviewed the paper. J.B. and D.S. generated the SARS-CoV-2 MA20 and reviewed the manuscript. T.C.M. reviewed the manuscript and provided advice. D.H. performed specific experiments, provided advice, and reviewed the paper. M.B. provided advice and reviewed the paper. B.C. and A.D. supervised the project, designed the experiments, and wrote the paper. B.C. performed specific experiments.

DECLARATION OF INTERESTS

J.G., K.K., N.R., and S.R. are employed by CureVac SE, which develops SARS-CoV-2 vaccines. The Friedrich-Loeffler-Institut receives funding for SARS-CoV-2 vaccine research by CureVac SE (Tübingen, Germany) and the RocketVax AG (Basel, Switzerland). M.B., D.H., and L.U. are part of a patent application for SARS-CoV-2 vaccines.

SUPPLEMENTAL INFORMATION

Supplemental information can be found online at <https://doi.org/10.1016/j.omtn.2024.102360>.

REFERENCES

- Regev-Yochay, G., Lustig, Y., Joseph, G., Gilboa, M., Barda, N., Gens, I., Indenbaum, V., Halpern, O., Katz-Likornik, S., Levin, T., et al. (2023). Correlates of protection against COVID-19 infection and intensity of symptomatic disease in vaccinated individuals exposed to SARS-CoV-2 in households in Israel (ICoFS): a prospective cohort study. *Lancet Microbe* 4, e309–e318. [https://doi.org/10.1016/S2666-5247\(23\)00012-5](https://doi.org/10.1016/S2666-5247(23)00012-5).
- Martín Pérez, C., Aguilar, R., Jiménez, A., Salmerón, G., Canyelles, M., Rubio, R., Vidal, M., Cuamba, I., Barrios, D., Díaz, N., et al. (2024). Correlates of protection and determinants of SARS-CoV-2 breakthrough infections 1 year after third dose vaccination. *BMC Med.* 22, 103. <https://doi.org/10.1186/s12916-024-03304-3>.
- Bitzenhofer, M., Suter-Riniker, F., Moor, M.B., Sidler, D., Horn, M.P., Gschwend, A., Staehelin, C., Rauch, A., Helbling, A., and Jörg, L. (2022). Humoral response to mRNA vaccines against SARS-CoV-2 in patients with humoral immunodeficiency disease. *PLoS One* 17, e0268780. <https://doi.org/10.1371/journal.pone.0268780>.
- Kashiwado, Y., Kimoto, Y., Ohshima, S., Sawabe, T., Irino, K., Nakano, S., Hiura, J., Yonekawa, A., Wang, Q., Doi, G., et al. (2024). Immunosuppressive therapy and humoral response to third mRNA COVID-19 vaccination with a six-month interval in rheumatic disease patients. *Rheumatology* 63, 725–733. <https://doi.org/10.1093/rheumatology/kead275>.
- Azar, J.H., Evans, J.P., Sikorski, M.H., Chakravarthy, K.B., McKenney, S., Carmody, I., Zeng, C., Teodorescu, R., Song, N.-J., Hamon, J.L., et al. (2023). Selective suppression of *de novo* SARS-CoV-2 vaccine antibody responses in patients with cancer on B cell-targeted therapy. *JCI Insight* 8, e163434. <https://doi.org/10.1172/jci.insight.163434>.
- Liu, J., Yu, J., McMahan, K., Jacob-Dolan, C., He, X., Giffin, V., Wu, C., Sciacca, M., Powers, O., Nampanya, F., et al. (2022). CD8 T cells contribute to vaccine protection against SARS-CoV-2 in macaques. *Sci. Immunol.* 7, eabq7647. <https://doi.org/10.1126/sciimmunol.abq7647>.
- Apostolidis, S.A., Kakara, M., Painter, M.M., Goel, R.R., Mathew, D., Lenzi, K., Rezk, A., Patterson, K.R., Espinoza, D.A., Kadri, J.C., et al. (2021). Cellular and humoral immune responses following SARS-CoV-2 mRNA vaccination in patients with multiple sclerosis on anti-CD20 therapy. *Nat. Med.* 27, 1990–2001. <https://doi.org/10.1038/s41591-021-01507-2>.
- Sun, K., Bhiman, J.N., Tempia, S., Kleynhans, J., Madzorera, V.S., Mkhize, Q., Kaldine, H., McMorrow, M.L., Wolter, N., Moyes, J., et al. (2024). SARS-CoV-2 correlates of protection from infection against variants of concern. *Nat. Med.* 30, 2805–2812. <https://doi.org/10.1038/s41591-024-03131-2>.

9. Fumagalli, V., Ravà, M., Marotta, D., Di Lucia, P., Bono, E.B., Giustini, L., De Leo, F., Casalgrandi, M., Monteleone, E., Mouro, V., et al. (2024). Antibody-independent protection against heterologous SARS-CoV-2 challenge conferred by prior infection or vaccination. *Nat. Immunol.* 25, 633–643. <https://doi.org/10.1038/s41590-024-01787-z>.
10. Israelow, B., Mao, T., Klein, J., Song, E., Menasche, B., Omer, S.B., and Iwasaki, A. (2021). Adaptive immune determinants of viral clearance and protection in mouse models of SARS-CoV-2. *Sci. Immunol.* 6, eabl4509. <https://doi.org/10.1126/sciimmunol.abl4509>.
11. Mason, D.Y., Jones, M., and Goodnow, C.C. (1992). Development and follicular localization of tolerant B lymphocytes in lysozyme/anti-lysozyme IgM/IgD transgenic mice. *Int. Immunol.* 4, 163–175. <https://doi.org/10.1093/intimm/4.2.163>.
12. Mozdanzowska, K., Furchner, M., Zharikova, D., Feng, J., and Gerhard, W. (2005). Roles of CD4+ T-cell-independent and -dependent antibody responses in the control of influenza virus infection: evidence for noncognate CD4+ T-cell activities that enhance the therapeutic activity of antiviral antibodies. *J. Virol.* 79, 5943–5951. <https://doi.org/10.1128/JVI.79.10.5943-5951.2005>.
13. McNamara, H.A., Idris, A.H., Sutton, H.J., Vistein, R., Flynn, B.J., Cai, Y., Wiehe, K., Lyke, K.E., Chatterjee, D., Kc, N., et al. (2020). Antibody Feedback Limits the Expansion of B Cell Responses to Malaria Vaccination but Drives Diversification of the Humoral Response. *Cell Host Microbe* 28, 572–585.e7. <https://doi.org/10.1016/j.chom.2020.07.001>.
14. Klarquist, J., Cross, E.W., Thompson, S.B., Willett, B., Aldridge, D.L., Caffrey-Carr, A.K., Xu, Z., Hunter, C.A., Getahun, A., and Kedl, R.M. (2021). B cells promote CD8 T cell primary and memory responses to subunit vaccines. *Cell Rep.* 36, 109591. <https://doi.org/10.1016/j.celrep.2021.109591>.
15. Dinno, K.H., Leist, S.R., Schäfer, A., Edwards, C.E., Martinez, D.R., Montgomery, S.A., West, A., Yount, B.L., Hou, Y.J., Adams, L.E., et al. (2020). A mouse-adapted model of SARS-CoV-2 to test COVID-19 countermeasures. *Nature* 586, 560–566. <https://doi.org/10.1038/s41586-020-2708-8>.
16. Beer, J., Crotta, S., Breithaupt, A., Ohnemus, A., Becker, J., Sachs, B., Kern, L., Llorian, M., Ebert, N., Labrousse, F., et al. (2022). Impaired immune response drives age-dependent severity of COVID-19. *J. Exp. Med.* 219, e20220621. <https://doi.org/10.1084/jem.20220621>.
17. Corleis, B., Hoffmann, D., Rauch, S., Fricke, C., Roth, N., Gergen, J., Kovacicova, K., Schlottau, K., Halwe, N.J., Ulrich, L., et al. (2023). Efficacy of an unmodified bivalent mRNA vaccine against SARS-CoV-2 variants in female small animal models. *Nat. Commun.* 14, 816. <https://doi.org/10.1038/s41467-023-36110-1>.
18. Anderson, K.G., Mayer-Barber, K., Sung, H., Beura, L., James, B.R., Taylor, J.J., Qunaj, L., Griffith, T.S., Vezys, V., Barber, D.L., and Masopust, D. (2014). Intravascular staining for discrimination of vascular and tissue leukocytes. *Nat. Protoc.* 9, 209–222. <https://doi.org/10.1038/nprot.2014.005>.
19. Kingstad-Bakke, B., Cleven, T., Bussan, H., Yount, B.L., Uraki, R., Iwatsuki-Horimoto, K., Koga, M., Yamamoto, S., Yotsuyanagi, H., Park, H., et al. (2023). Airway surveillance and lung viral control by memory T cells induced by COVID-19 mRNA vaccine. *JCI Insight* 8, e172510. <https://doi.org/10.1172/jci.insight.172510>.
20. Tai, W., Feng, S., Chai, B., Lu, S., Zhao, G., Chen, D., Yu, W., Ren, L., Shi, H., Lu, J., et al. (2023). An mRNA-based T-cell-inducing antigen strengthens COVID-19 vaccine against SARS-CoV-2 variants. *Nat. Commun.* 14, 2962. <https://doi.org/10.1038/s41467-023-38751-8>.
21. Hassan, A.O., Case, J.B., Winkler, E.S., Thackray, L.B., Kafai, N.M., Bailey, A.L., McCune, B.T., Fox, J.M., Chen, R.E., Alsoussi, W.B., et al. (2020). A SARS-CoV-2 Infection Model in Mice Demonstrates Protection by Neutralizing Antibodies. *Cell* 182, 744–753.e4. <https://doi.org/10.1016/j.cell.2020.06.011>.
22. Ying, B., Darling, T.L., Desai, P., Liang, C.-Y., Dmitriev, I.P., Soudani, N., Bricker, T., Kashentseva, E.A., Harastani, H., Raju, S., et al. (2024). Mucosal vaccine-induced cross-reactive CD8+ T cells protect against SARS-CoV-2 XBB.1.5 respiratory tract infection. *Nat. Immunol.* 25, 537–551. <https://doi.org/10.1038/s41590-024-01743-x>.
23. Uddäck, I., Michalets, S.E., Saha, A., Mattingly, C., Kost, K.N., Williams, M.E., Lawrence, L.A., Hicks, S.L., Lowen, A.C., Ahmed, H., et al. (2024). Prevention of respiratory virus transmission by resident memory CD8+ T cells. *Nature* 626, 392–400. <https://doi.org/10.1038/s41586-023-06937-1>.
24. Ramirez, S.I., Faraji, F., Hills, L.B., Lopez, P.G., Goodwin, B., Stacey, H.D., Sutton, H.J., Hastie, K.M., Saphire, E.O., Kim, H.J., et al. (2024). Immunological memory diversity in the human upper airway. *Nature* 632, 630–636. <https://doi.org/10.1038/s41586-024-07748-8>.
25. Cao, K.T., Cobos-Urbe, C., Knight, N., Jonnalagadda, R., Robinette, C., Jaspers, I., and Rebuli, M.E. (2023). SARS-CoV-2 mRNA vaccination induces an intranasal mucosal response characterized by neutralizing antibodies. *J. Allergy Clin. Immunol. Glob.* 2, 100129. <https://doi.org/10.1016/j.jacig.2023.100129>.
26. Sano, K., Bhavsar, D., Singh, G., Floda, D., Srivastava, K., Gleason, C., Carreño, J.M., PARIS Study Group, Simon, V., and Krammer, F. (2022). SARS-CoV-2 vaccination induces mucosal antibody responses in previously infected individuals. *Nat. Commun.* 13, 5135. <https://doi.org/10.1038/s41467-022-32389-8>.
27. Sheikh-Mohamed, S., Isho, B., Chao, G.Y.C., Zuo, M., Cohen, C., Lustig, Y., Nahass, G.R., Salomon-Shulman, R.E., Blacker, G., Fazel-Zarandi, M., et al. (2022). Systemic and mucosal IgA responses are variably induced in response to SARS-CoV-2 mRNA vaccination and are associated with protection against subsequent infection. *Mucosal Immunol.* 15, 799–808. <https://doi.org/10.1038/s41385-022-00511-0>.
28. Puhach, O., Bellon, M., Adea, K., Bekliz, M., Hosszu-Fellous, K., Sattonnet, P., Hulo, N., Kaiser, L., Eckerle, I., and Meyer, B. (2023). SARS-CoV-2 convalescence and hybrid immunity elicits mucosal immune responses. *EBioMedicine* 98, 104893. <https://doi.org/10.1016/j.ebiom.2023.104893>.
29. Bladh, O., Aguilera, K., Marking, U., Kihlgren, M., Greilert Norin, N., Smed-Sörensen, A., Sällberg Chen, M., Klingström, J., Blom, K., Russell, M.W., et al. (2024). Comparison of SARS-CoV-2 spike-specific IgA and IgG in nasal secretions, saliva and serum. *Front. Immunol.* 15, 1346749. <https://doi.org/10.3389/fimmu.2024.1346749>.
30. Cohen, J.I., Dropulic, L., Wang, K., Gangler, K., Morgan, K., Liepshutz, K., Krogmann, T., Ali, M.A., Qin, J., Wang, J., et al. (2023). Comparison of Levels of Nasal, Salivary, and Plasma Antibody to Severe Acute Respiratory Syndrome Coronavirus 2 During Natural Infection and After Vaccination. *Clin. Infect. Dis.* 76, 1391–1399. <https://doi.org/10.1093/cid/ciac934>.
31. Ishizaka, A., Koga, M., Mizutani, T., Uraki, R., Yamayoshi, S., Iwatsuki-Horimoto, K., Yamamoto, S., Imai, M., Tsutsumi, T., Suzuki, Y., et al. (2023). Antibody induction and immune response in nasal cavity by third dose of SARS-CoV-2 mRNA vaccination. *Virol. J.* 20, 146. <https://doi.org/10.1186/s12985-023-02113-z>.
32. Carr, E.J., Dowgier, G., Greenwood, D., Herman, L.S., Hobbs, A., Ragno, M., Stevenson-Leggett, P., Gahir, J., Townsley, H., Harvey, R., et al. (2024). SARS-CoV-2 mucosal neutralising immunity after vaccination. *Lancet Infect. Dis.* 24, e4–e5. [https://doi.org/10.1016/S1473-3099\(23\)00705-3](https://doi.org/10.1016/S1473-3099(23)00705-3).
33. Hoffmann, D., Corleis, B., Rauch, S., Roth, N., Mühle, J., Halwe, N.J., Ulrich, L., Fricke, C., Schön, J., Kraft, A., et al. (2021). CVnCoV and CV2CoV protect human ACE2 transgenic mice from ancestral B BavPat1 and emerging B.1.351 SARS-CoV-2. *Nat. Commun.* 12, 4048. <https://doi.org/10.1038/s41467-021-24339-7>.
34. Roth, N., Schön, J., Hoffmann, D., Thran, M., Thess, A., Mueller, S.O., Petsch, B., and Rauch, S. (2022). Optimised Non-Coding Regions of mRNA SARS-CoV-2 Vaccine CV2CoV Improves Homologous and Heterologous Neutralising Antibody Responses. *Vaccines* 10, 1251. <https://doi.org/10.3390/vaccines10081251>.
35. Fricke, C., Pfaff, F., Ulrich, L., Halwe, N.J., Schön, J., Timm, L., Hoffmann, W., Rauch, S., Petsch, B., Hoffmann, D., et al. (2023). SARS-CoV-2 variants of concern elicit divergent early immune responses in hACE2 transgenic mice. *Eur. J. Immunol.* 53, e2250332. <https://doi.org/10.1002/eji.202250332>.
36. Wernike, K., Aeberscher, A., Michelitsch, A., Hoffmann, D., Freuling, C., Balkema-Buschmann, A., Graaf, A., Müller, T., Osterrieder, N., Rissmann, M., et al. (2021). Multi-species ELISA for the detection of antibodies against SARS-CoV-2 in animals. *Transbound. Emerg. Dis.* 68, 1779–1785. <https://doi.org/10.1111/tbed.13926>.

Supplemental information

mRNA vaccine-induced IgG mediates nasal

SARS-CoV-2 clearance in mice

Charlie Fricke, Lorenz Ulrich, Jana Kochmann, Janina Gergen, Kristina Kovacikova, Nicole Roth, Julius Beer, Daniel Schnepf, Thomas C. Mettenleiter, Susanne Rauch, Benjamin Petsch, Donata Hoffmann, Martin Beer, Björn Corleis, and Anca Dorhoi

Supplemental information:

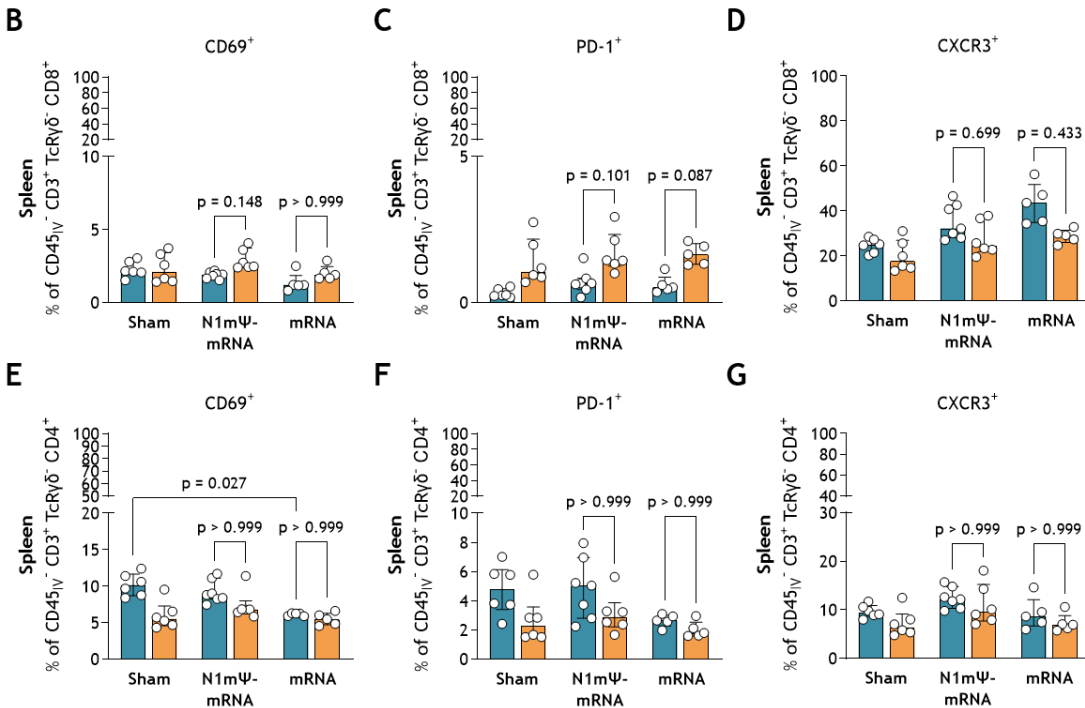
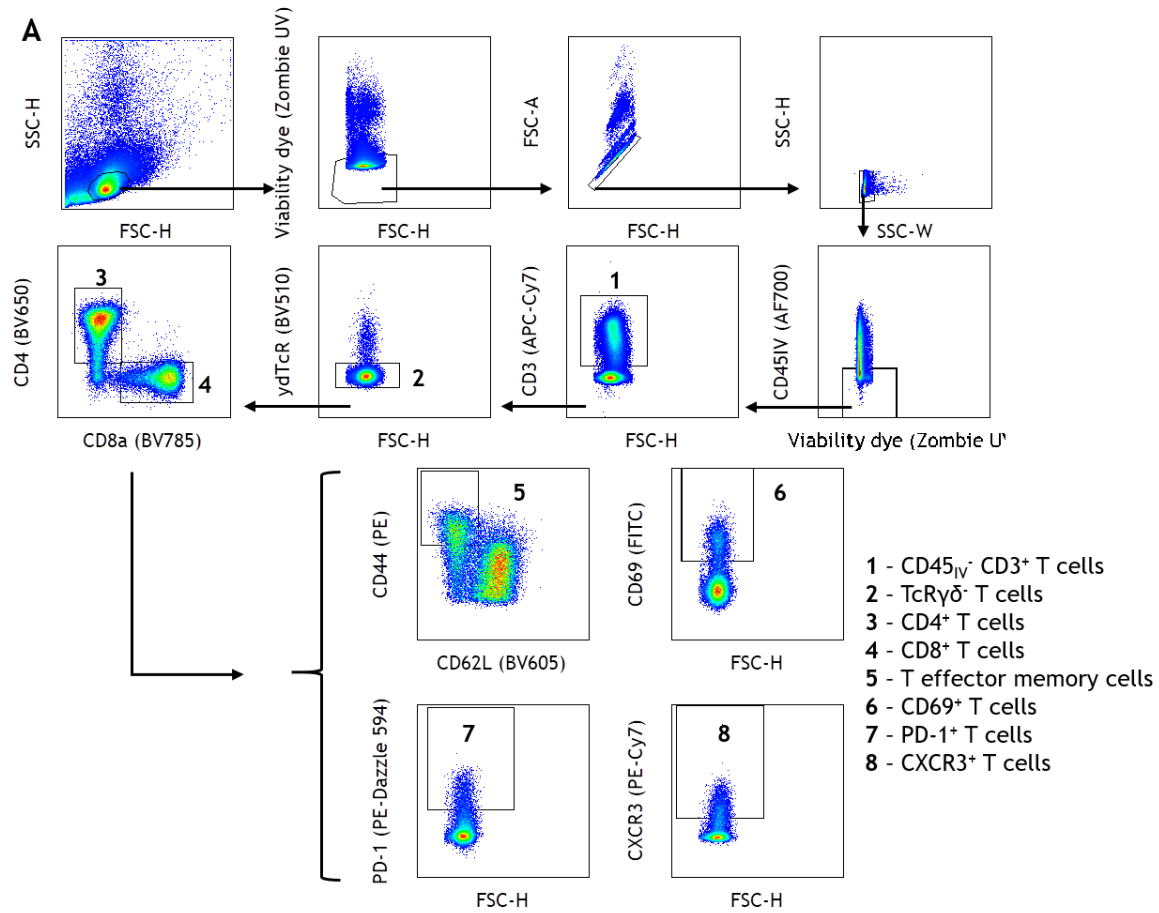


Fig. S1 | Flow cytometry gating strategy and analysis for CD45_{IV}⁻ T cells in the lungs and spleen. **A:** Lung and spleen lymphocytes were identified using FSC-H against SSC-H gating. FSH-H/FSC-A and SSC-W/SSC-H gating eliminated doublets. The fixable live/dead viability dye (Zombie UV, BioLegend GmbH) was used to exclude dead cells. During lethal anaesthesia, an intravenous injection of anti-mouse CD45 antibodies was administered to distinguish parenchymal (CD45_{IV}⁻) from vascular cells (CD45_{IV}⁺). Before gating on CD4⁺ helper T cells and CD8⁺ cytotoxic T cells, CD3⁺ γδTCR⁺ T cells were excluded. Effector memory T cells (T_{em}) were characterized as CD44^{hi} and CD62L⁻. The flow plots were created from one representative mouse sample. **B-G:** Pre-challenge CD4⁺ and CD8⁺ T cells from the spleen of mice (d56) were analyzed for CD69 (**B and E**), PD-1 (**C and F**) and CXCR3 (**D and G**) expression. Each data point represents one animal. n = 6 per vaccine and mouse group. n = 7 for N1mΨ-mRNA WT. n = 5 for mRNA. The median with the interquartile range is displayed. p Values were determined by nonparametric one-way ANOVA and Dunn's multiple comparison test.

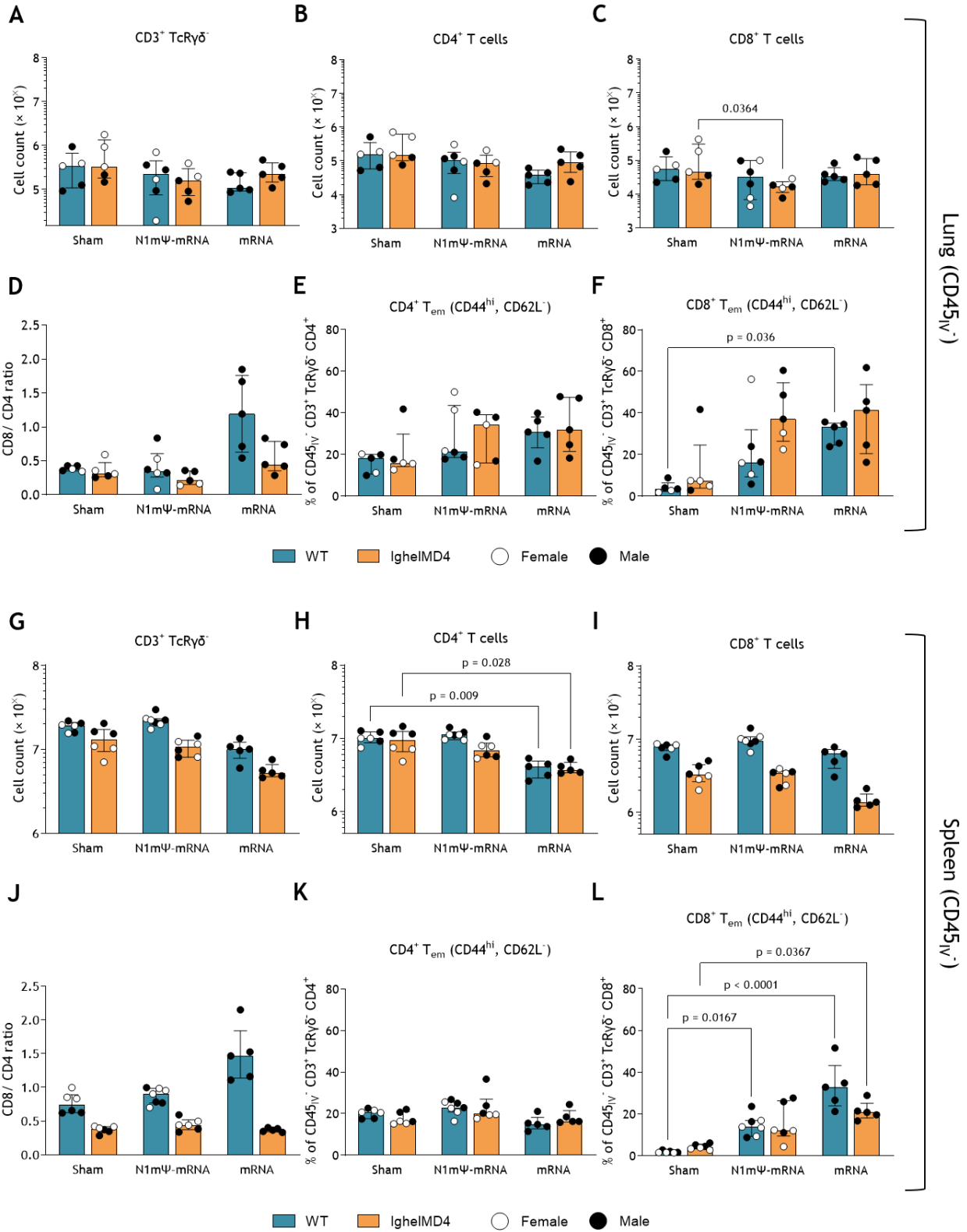


Fig. S2 | Analysis of lung and spleen T cell populations in mRNA-vaccinated WT and IgheIMD4 mice pre-challenge infection (d56). A-C: Counts of T cell populations in the lungs gated on CD45^{IV-}, CD3⁺, TcRγδ⁻ (A)

and CD4⁺ (**B**) or CD8⁺ (**C**). **D**: CD8/ CD4 T cell ratio in the lungs. **E-F**: CD4⁺ (**E**) and CD8⁺ (**F**) T_{em} cells in the lungs. **G-I**: Counts of T cell populations in the spleen gated on CD45^{IV}⁻, CD3⁺, TcRγδ⁻ and CD4⁺ (**H**) or CD8⁺ (**I**). **J**: CD8/ CD4 T cell ratio in the spleen. **K-L**: CD4⁺ (**K**) and CD8⁺ (**L**) T_{em} cells in the spleen. **A-F**: Number of animals: n = 5 per group, n = 6 for N1mΨ-mRNA WT. **G-L**: Number of animals: n = 6 per group, n = 7 for N1mΨ-mRNA WT, n = 5 for mRNA WT and ighelMD4. **A-L**: p values were determined by nonparametric one-way ANOVA and Dunn's multiple comparison test. Each data point represents one female (white dot) or male (black dot) animal.

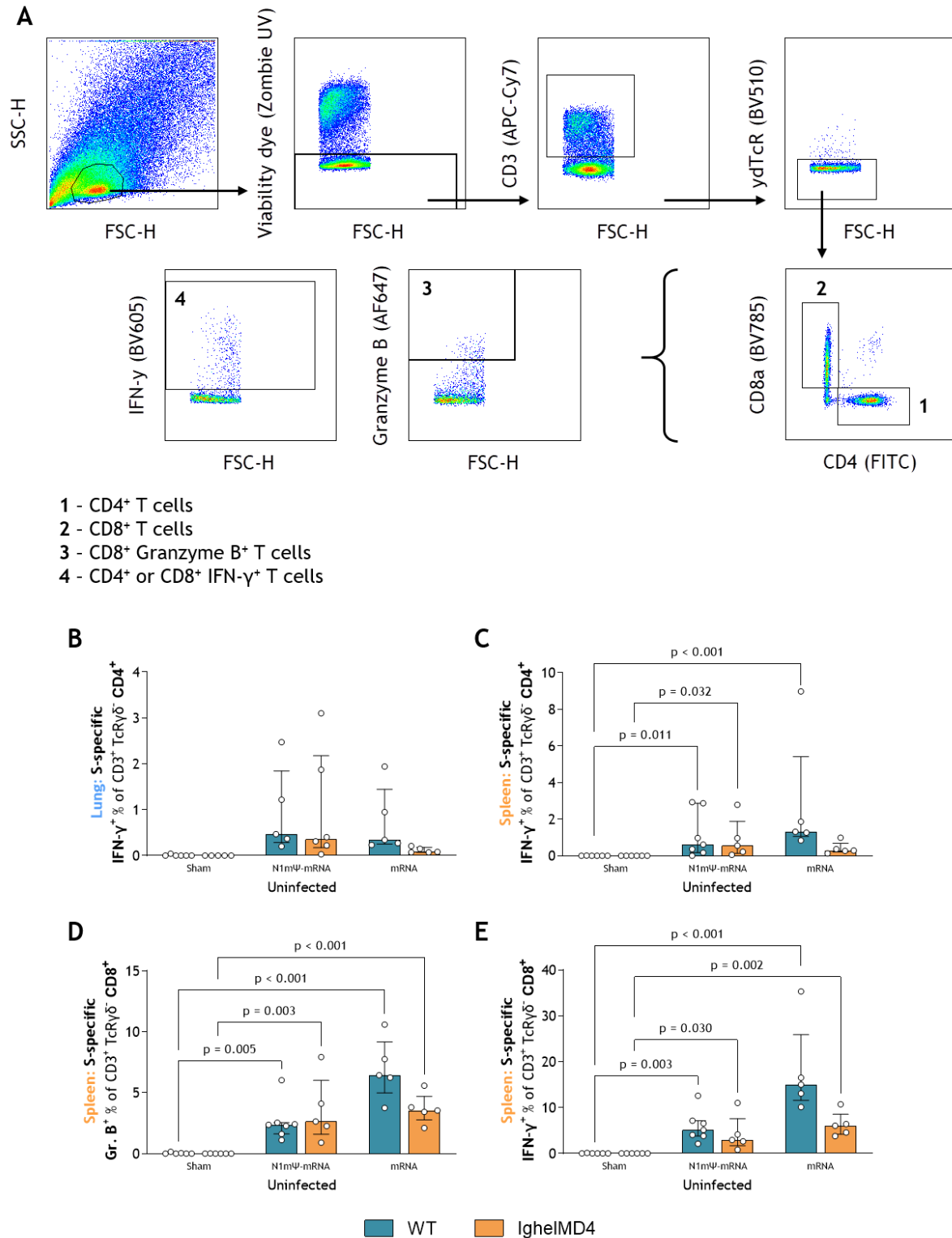


Fig. S3 | Analysis of S-specific lung and spleen T cells after vaccination pre-challenge infection. A: Flow cytometry gating strategy for S-specific T cell responses. Lung and spleen lymphocytes were identified by FSC-H against SSC-H gating. Dead cells were excluded using the fixable live/dead viability

dye (Zombie UV, BioLegend GmbH) before gating on CD3⁺ T cells. $\gamma\delta$ TCR⁺ T cells were excluded. Expression analysis of Granzyme B and IFN- γ was performed for CD8⁺ and CD4⁺ T cells. Flow plots were generated from one representative sample. **B-E:** Single-cell suspensions obtained from the lungs and spleen of mice were restimulated in vitro with S peptides. The percentage of CD8⁺ T cells that expressed Granzyme B (**D**) or CD4⁺ and CD8⁺ T cells that expressed IFN- γ (**B, C and E**) in the lungs (**B**) and spleen (**C-E**) at day 56 is presented. The values were obtained by subtracting percentage [unstimulated] from percentage [S peptide stimulated]. Each data point represents one animal. The median with the interquartile range is displayed. p Values were determined by nonparametric one-way ANOVA and Dunn's multiple comparison test. **B:** n = 5 per vaccine and mouse group. n = 6 for Sham WT and N1m Ψ -mRNA IghelMD4. **C-E:** n = 5 per vaccine and mouse group. n = 6 for Sham, n = 7 for N1m Ψ -mRNA WT, n = 5 for N1m Ψ -mRNA IghelMD4 and mRNA.

Values were determined by nonparametric one-way ANOVA and Dunn's multiple comparison test. **A and B:** Each data point represents one animal.

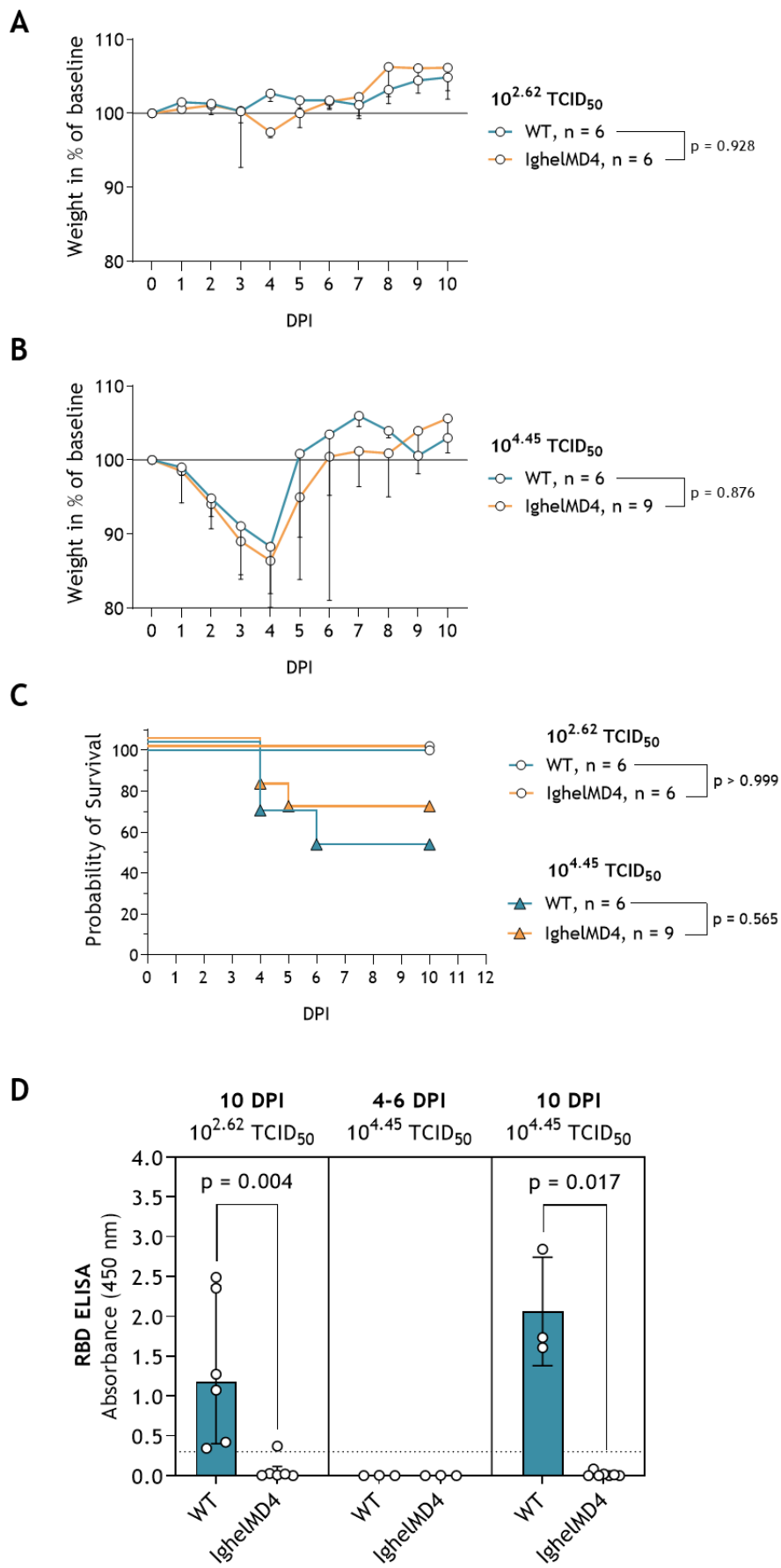
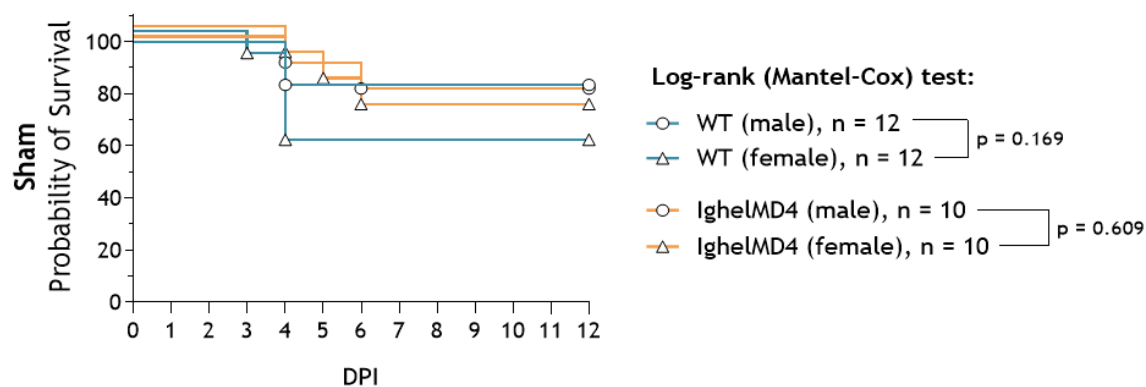
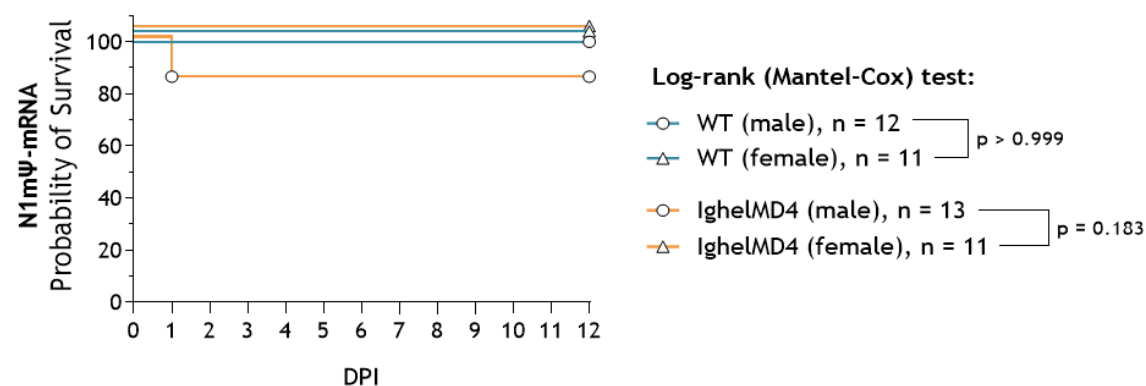


Fig. S5 | Prior dose finding experiment. A and B: Weight changes of WT and IghelMD4 mice intranasally infected with $10^{2.62}$ (**A**) or $10^{4.45}$ TCID₅₀ (**B**) of SARS-CoV-2 MA20 until 10 DPI. Each data point represents the median with the interquartile range. p Values were determined by two-way ANOVA (mixed effects analysis). **A:** n = 6 for WT, n = 6 for IghelMD4. **B:** Number of animals: n = 6 for WT, n = 9 for IghelMD4. **C:** Survival analysis for WT and IghelMD4 mice infected with $10^{2.62}$ or $10^{4.45}$ TCID₅₀ of SARS-CoV-2 MA20 up to 10 DPI. p Values were determined by direct curve comparison (Kaplan Meier) using the log-rank (Mantel-Cox) test. **D:** RBD ELISA of WT and IghelMD4 mice infected with $10^{2.62}$ or $10^{4.45}$ TCID₅₀ of SARS-CoV-2 MA20. The dotted line (...) represents the cutoff for seroconversion (OD = 0.3). Number of animals: n = 6 for WT and IghelMD4 ($10^{2.62}$ TCID₅₀), n = 3 for WT and IghelMD4 ($10^{4.45}$ TCID₅₀, 4-6 DPI), n = 3 for WT ($10^{4.45}$ TCID₅₀, 10 DPI), n = 7 for IghelMD4 ($10^{4.45}$ TCID₅₀, 10 DPI). Each data point represents one animal. The median with the interquartile range is displayed. p values were determined by the nonparametric Mann-Whitney test.

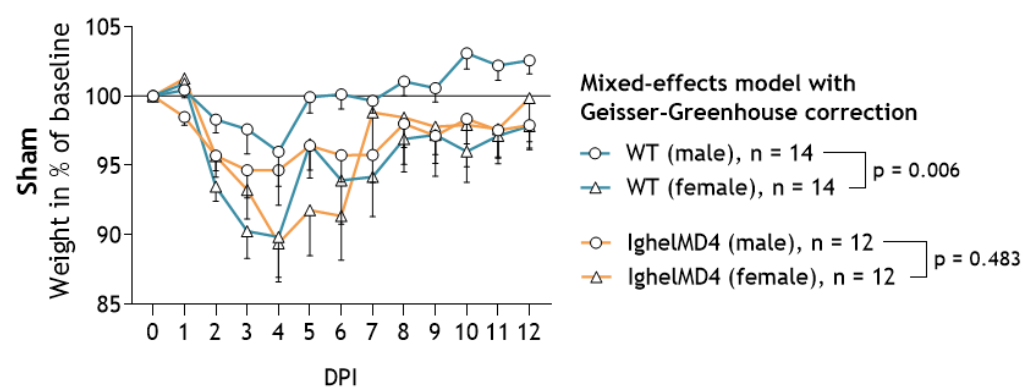
A



B



C



D

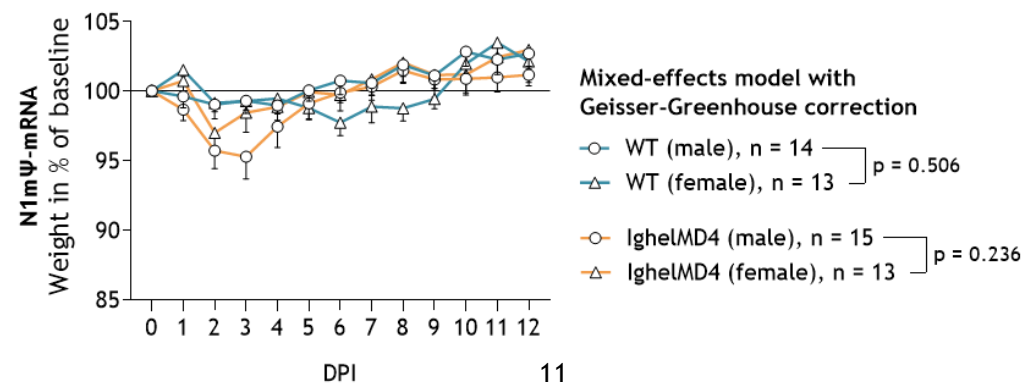


Fig. S6 | Sex-based analysis of survival and weight changes upon infection with SARS-CoV-2 MA20. A and B: Sex-based survival analysis for Sham (**A**) and N1m Ψ -mRNA (**B**) vaccinated WT and IghelMD4 mice after infection with SARS-CoV-2 MA20 up to 12 DPI. p Values were determined by direct curve comparison (Kaplan Meier) using the log-rank (Mantel-Cox) test. **A:** Number of animals: n = 12 for male and female WT, n = 10 for male and female IghelMD4. **B:** Number of animals: n = 12 for male and n = 11 for female WT, n = 13 for male IghelMD4, n = 11 for female IghelMD4. **C and D:** Sex-based analysis of weight changes until 12 DPI for Sham (**C**) and N1m Ψ -mRNA (**D**) vaccinated WT and IghelMD4 mice. The data set passed the D'Agostino-Pearson normality test ($\alpha = 0.05$). Each data point represents the mean with SEM. p Values were determined by two-way ANOVA (mixed effects analysis). **C:** Number of animals: n = 14 for male and female WT, n = 12 for male and female IghelMD4. **D:** Number of animals: n = 14 for male WT, n = 13 for female WT, n = 15 for male IghelMD4, n = 13 for female IghelMD4. **A-D:** Exclusion of animals which reached the predetermined study endpoint at 3 DPI (n = 4 per group for Sham and N1m Ψ -mRNA) from survival analysis caused differences in the number of animals in survival (**A and B**) and weight change plots (**C and D**) for each group.

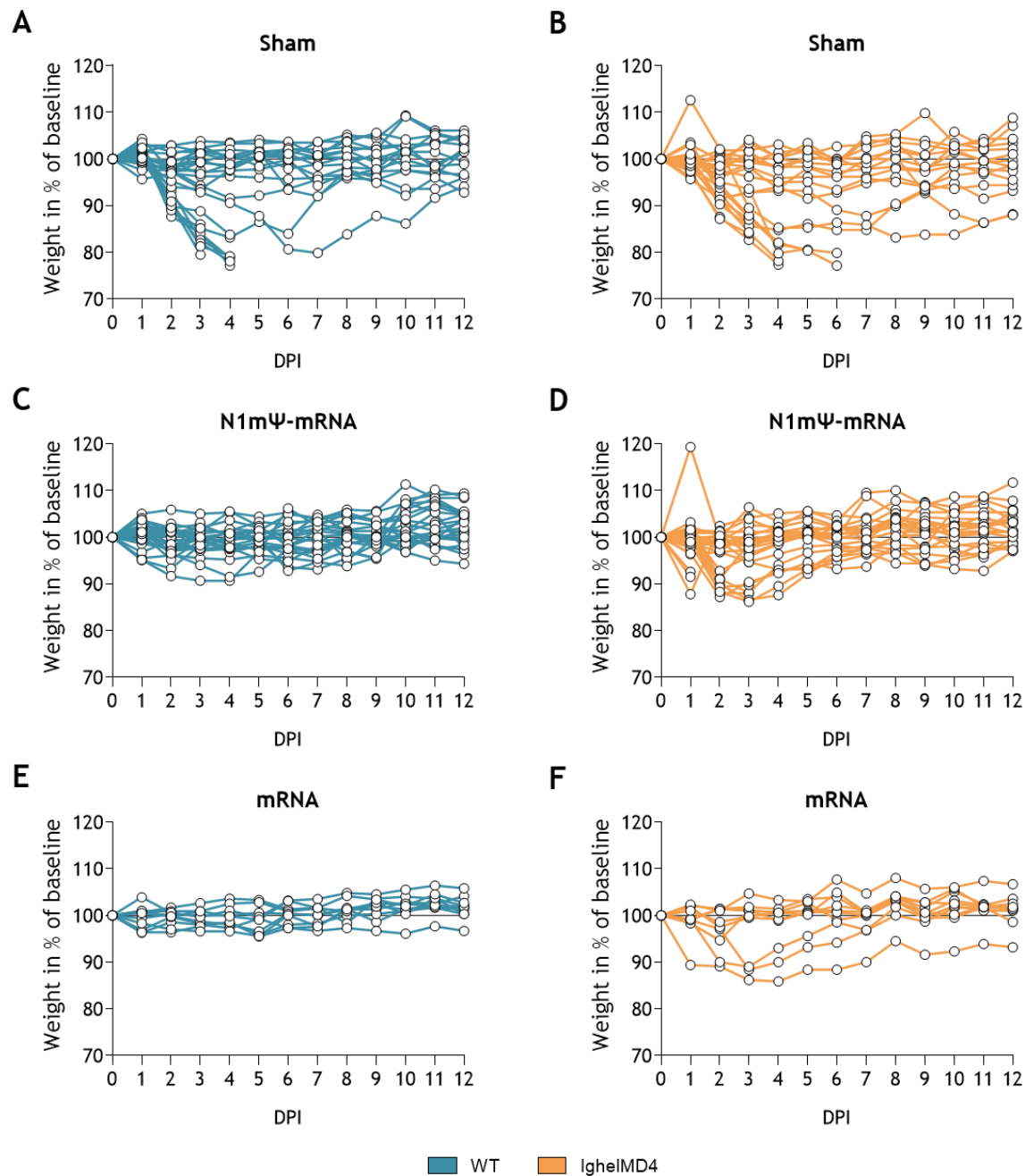


Fig. S7 | Weight changes of individual mice upon SARS-CoV-2 MA20 infection. **A-F:** Individual mice vaccinated with NaCl (Sham) (**A and B**), N1mΨ-mRNA (**C and D**) or mRNA (**E and F**) were challenged with SARS-CoV-2 MA20 and monitored for weight changes up to 12 DPI. Each line represents one animal. **A-F:** Number of animals: n = 28 (**A**), n = 24 (**B**), n = 27 (**C**), n = 28 (**D**), n = 10 (**E**) and n = 10 (**F**).

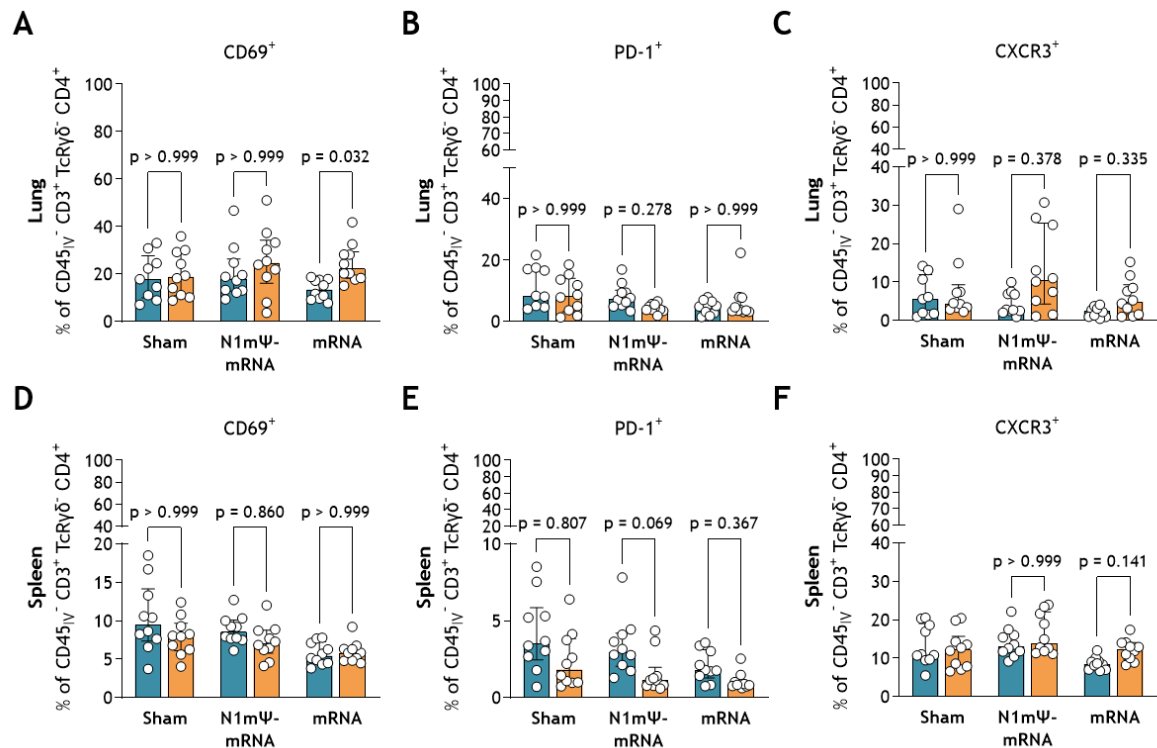


Fig. S8 | Expression analysis of activation and homing markers of lung and spleen T cells 12 DPI. A-F: Post-challenge CD4⁺ and CD8⁺ T cells from the lungs (A-C) and spleen (D-F) of mice 12 DPI were analyzed for CD69 (A and D), PD-1 (B and E) and CXCR3 (C and F) expression using flow cytometry. Each data point represents one animal. n = 10 per vaccine and mouse group, n = 9 for Sham WT (lungs). The median with the interquartile range is displayed. p Values were determined by nonparametric one-way ANOVA and Dunn's multiple comparison test.

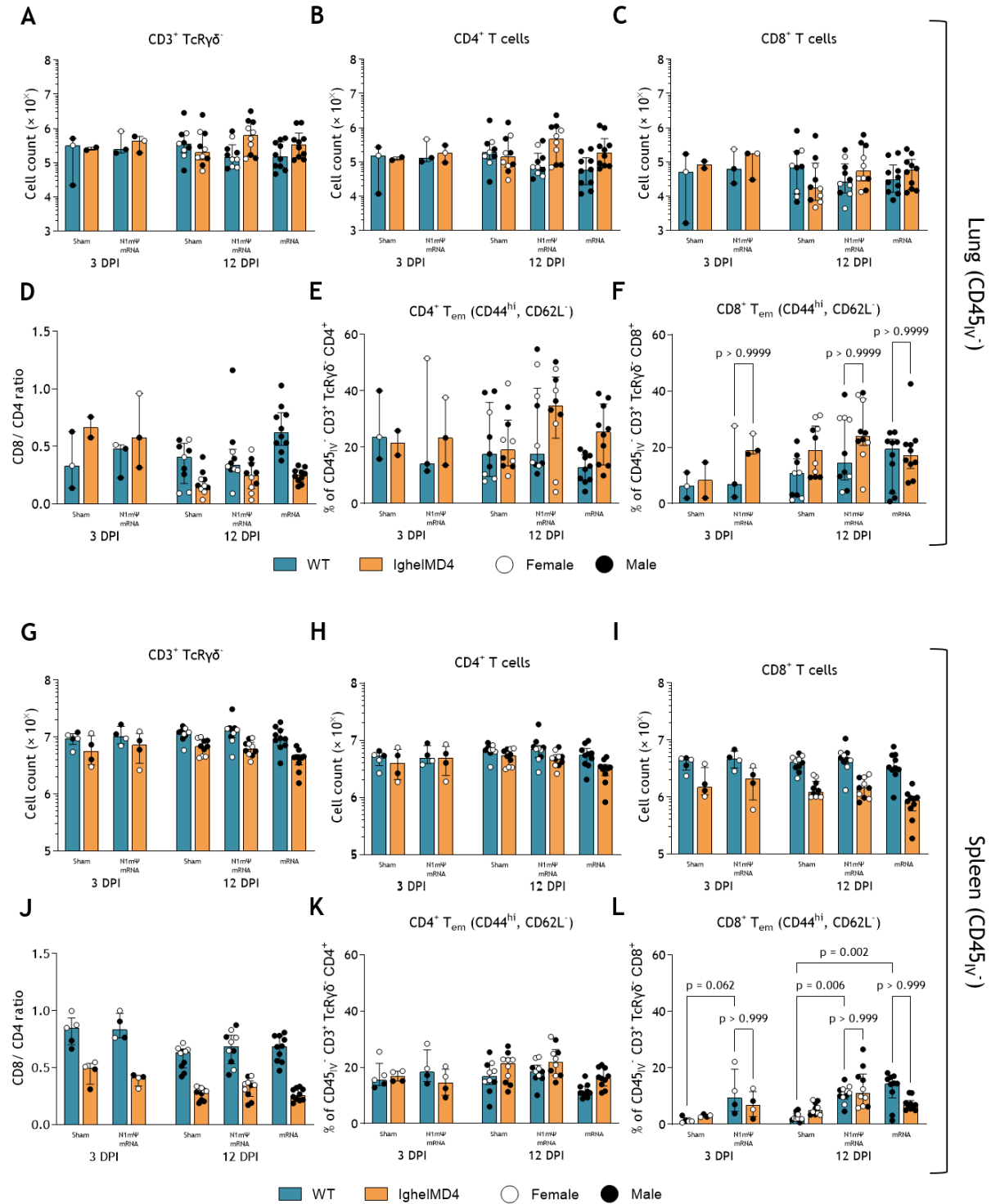


Fig. S9 | Analysis of lung and spleen T cell populations in mRNA-vaccinated WT and IghelMD4 mice post-challenge infection at 3 and 12 DPI. A-C: Counts of T cell populations in the lungs gated on CD45^{IV}-, CD3⁺, TcRγδ⁻ (A) and CD4⁺ (B) or CD8⁺ (C). **D:** CD8/CD4 T cell ratio in the lungs. **E-F:** CD4⁺ (E) and CD8⁺ (F) T_{em} cells in the lungs. **G-I:** Counts of T cell

populations in the spleen gated on CD45^{IV-}, CD3⁺, TcR $\gamma\delta$ ⁻ (**G**) and CD4⁺ (**H**) or CD8⁺ (**I**). **J**: CD8/ CD4 T cell ratio in the spleen. **K-L**: CD4⁺ (**K**) and CD8⁺ (**L**) T_{em} cells in the spleen. **A-F**: Number of animals: n = 3 per group for 3 DPI, n = 2 for Sham IghelMD4 (3 DPI), n = 10 per group for 12 DPI, n = 9 for Sham WT (12 DPI). **G-L**: Number of animals: n = 4 per group for 3 DPI, n = 5 for Sham WT (3 DPI), n = 10 per group for 12 DPI. **A-L**: p values were determined by nonparametric one-way ANOVA and Dunn's multiple comparison test. Each data point represents one female (white dot) or male (black dot) animal.

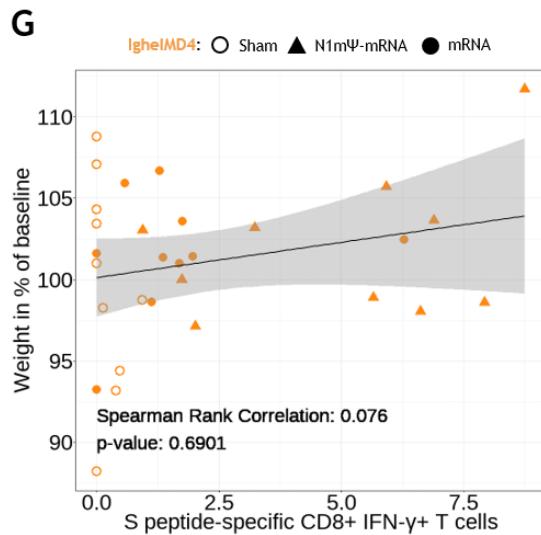
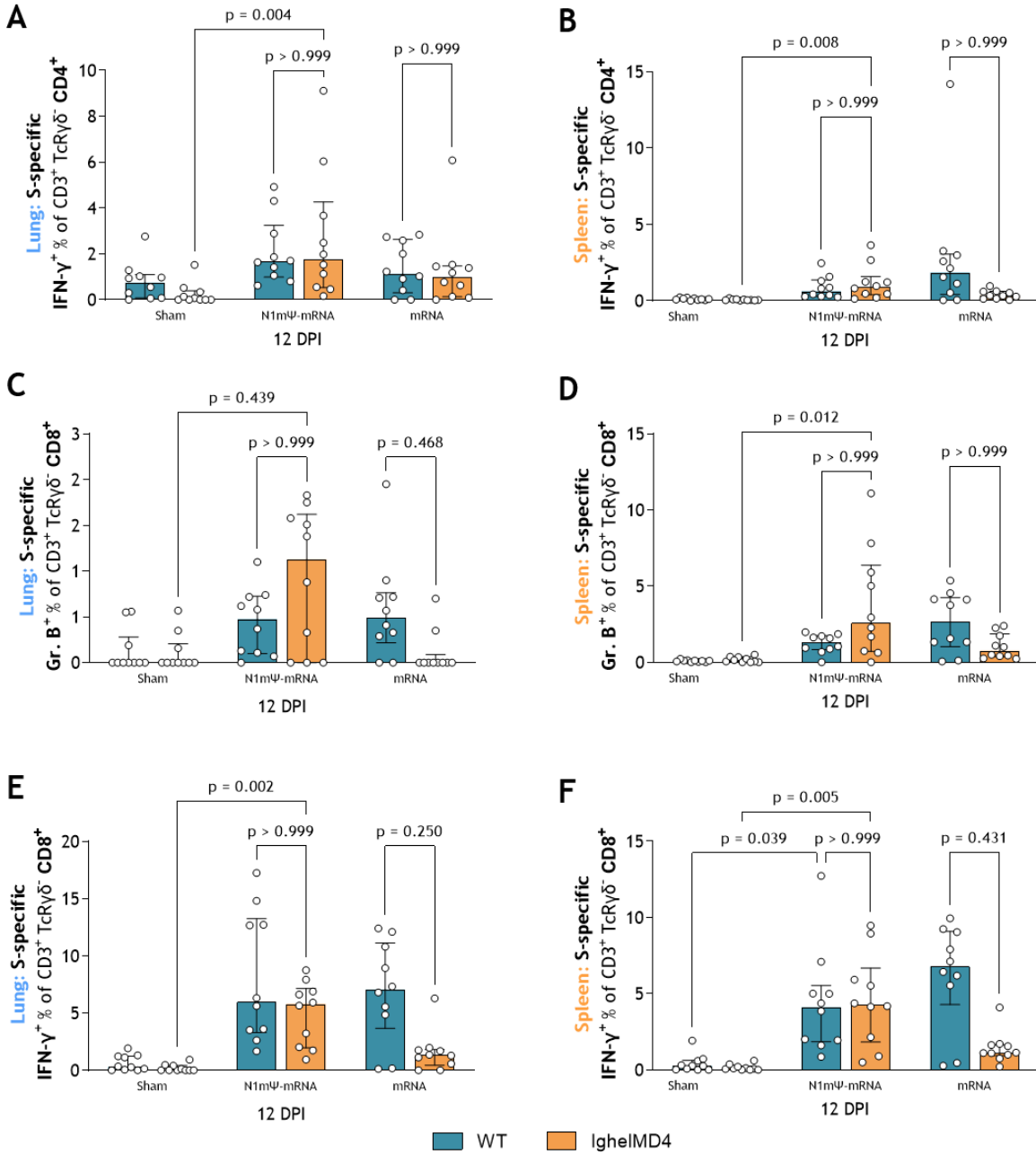


Fig. S10 | Analysis of S-specific lung and spleen T cells after vaccination post-challenge infection at 12 DPI. A-F: Single-cell suspensions obtained from the lungs and spleen of mice were restimulated in vitro with S peptides. The percentage of CD4⁺ (**A and B**) or CD8⁺ (**C-F**) T cells that expressed Granzyme B (**C and D**) or IFN- γ (**A, B, E and F**) in the lungs (**A, C and E**) and spleen (**B, D and F**) at 12 DPI is presented. Number of animals: n = 10 per group. The values were obtained by subtracting percentage [unstimulated] from percentage [S peptide stimulated]. The median with the interquartile range is displayed. p Values were determined by nonparametric one-way ANOVA and Dunn's multiple comparison test. **G:** Linear regression and correlation of S peptide-specific CD8⁺ IFN- γ ⁺ T cells with weight on the day of death for IghelMD4 mice at 12 DPI. Number of animals: n = 10 per group. Two-tailed Spearman rank correlation was performed with R (version 4.3.2) in R studio (2023.12.1 build 402) using cor.test(). The regression line was added using geom_smooth() and the linear model (lm) method within the ggplot2 visualization package. The grey area represents the 95 % confidence interval. **A-G:** Each data point represents one animal.

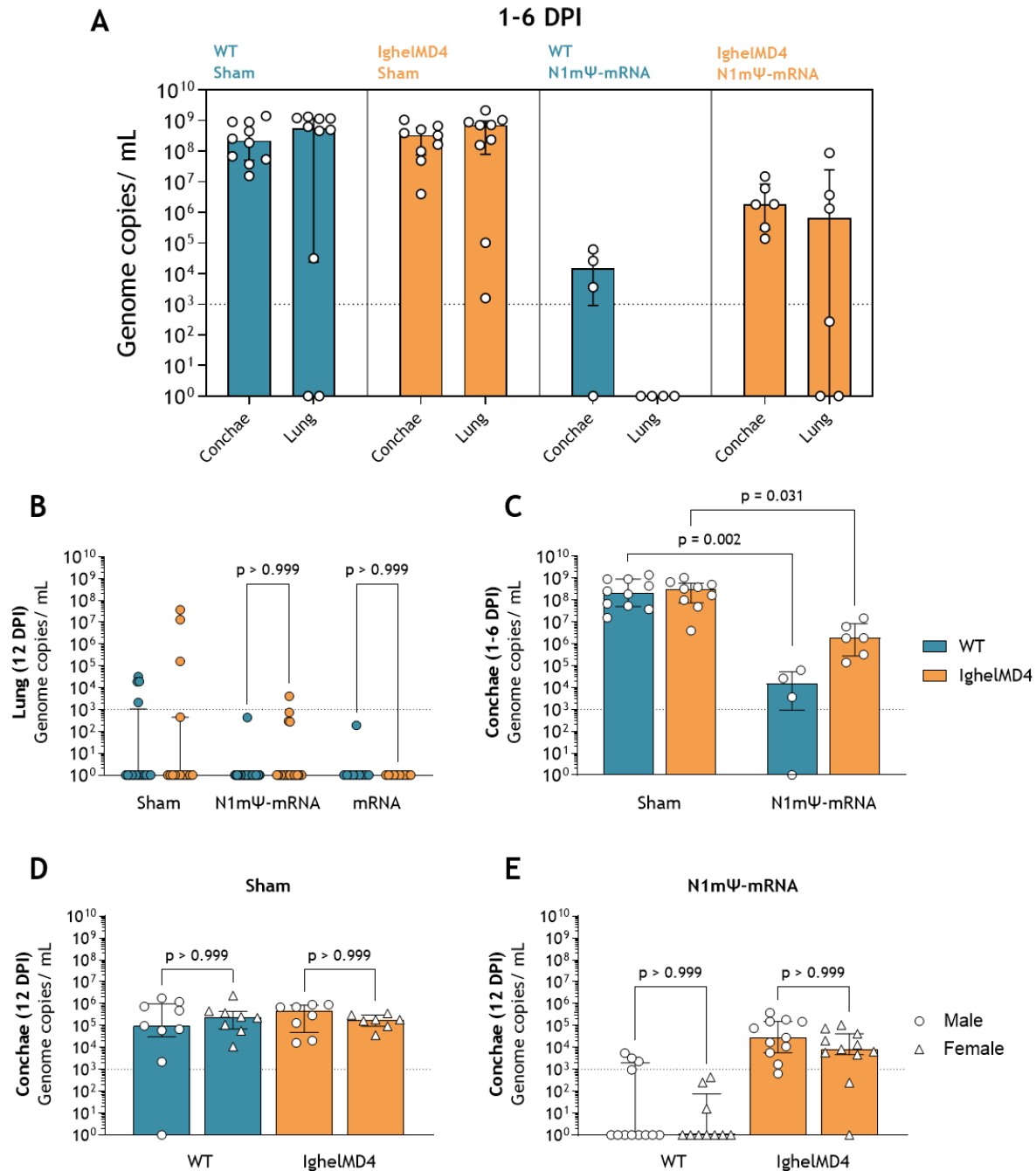


Fig. S11 | Viral loads of WT and IgheIMD4 mice infected with SARS-CoV-2 MA20. A: Viral loads in the conchae and lungs of Sham or N1mΨ-mRNA-vaccinated mice at 1-6 DPI. Number of animals: $n = 10$ for Sham WT, $n = 9$ for Sham IgheIMD4, $n = 4$ for N1mΨ-mRNA WT, $n = 6$ for N1mΨ-mRNA IgheIMD4. **B:** Lung viral loads at 12 DPI in WT and IgheIMD4 mice vaccinated with NaCl (Sham), N1mΨ-mRNA or mRNA. Number of animals: $n = 17$ for Sham WT, $n = 15$ for Sham IgheIMD4, $n = 23$ for N1mΨ-mRNA WT, $n = 22$

for N1mΨ-mRNA IghelMD4, n = 10 for mRNA WT and IghelMD4. **C:** Conchae viral loads at 1-6 DPI in WT and IghelMD4 mice vaccinated with NaCl (Sham) or N1mΨ-mRNA. Number of animals: n = 10 for Sham WT, n = 9 for Sham IghelMD4, n = 4 for N1mΨ-mRNA WT, n = 6 for N1mΨ-mRNA IghelMD4. **D and E:** Sex-based analysis of conchae (**D**) and lung (**E**) viral loads 12 DPI. **D:** Number of animals: n = 9 for male WT, n = 8 for male IghelMD4, n = 8 for female WT, n = 7 for female IghelMD4. **E:** Number of animals: n = 12 for male WT, n = 11 for male IghelMD4, n = 10 for female WT, n = 11 for female IghelMD4. **A-E:** The detection limit was set at 10^3 vRNA copies per mL, represented by a dotted line (...). Each data point represents one animal. **B-E:** p Values were determined by nonparametric one-way ANOVA and Dunn's multiple comparison test.

Table S1 | Number of mice per sex, genotype and vaccine group used pre- and post-challenge infection.

| Time point | n = | Sex | Genotype | Vaccine |
|----------------|--------------------------|-----|----------|-----------|
| Pre-challenge | 3 | M | WT | Sham |
| | 3 | | WT | N1mΨ-mRNA |
| | 3 | | IghelMD4 | Sham |
| | 3 | | IghelMD4 | N1mΨ-mRNA |
| | 3 | F | WT | Sham |
| | 3 | | WT | N1mΨ-mRNA |
| | 3 | | IghelMD4 | Sham |
| | 3 | | IghelMD4 | N1mΨ-mRNA |
| | 5 | M | WT | mRNA |
| | 5 | | IghelMD4 | mRNA |
| | <u>Total: 34</u> | | | |
| Post-challenge | 14 | M | WT | Sham |
| | 14 | | WT | N1mΨ-mRNA |
| | 12 | | IghelMD4 | Sham |
| | 15 | | IghelMD4 | N1mΨ-mRNA |
| | 14 | F | WT | Sham |
| | 14 | | WT | N1mΨ-mRNA |
| | 12 | | IghelMD4 | Sham |
| | 13 | | IghelMD4 | N1mΨ-mRNA |
| | 10 | M | WT | mRNA |
| | 10 | | IghelMD4 | mRNA |
| | <u>Total: 128</u> | | | |

Table S2 | Antibodies used for T cell flow cytometry staining.

| Panel | Molecule | Fluorochrome | Isotype | Clone | Company | Cat # | Amount/ Dilution factor |
|---|-------------|-----------------------|----------------------|--------------|-------------------------|------------|----------------------------|
| T cell surface receptor analysis | CD45 (i.v.) | Alexa Fluor® 700 | Rat IgG2b, κ | 30-F11 | BioLegend GmbH | 103127 | 3 µg in 100 µl PBS |
| | CD3 | APC/Cyanine7 | Rat IgG2b, κ | 17A2 | BioLegend GmbH | 100221 | 100 |
| | CD4 | Brilliant Violet 650™ | Rat IgG2a, κ | RM4-5 | BioLegend GmbH | 100545 | 150 |
| | CD8a | Brilliant Violet 785™ | Rat IgG2a, κ | 53-6.7 | BioLegend GmbH | 100749 | 100 |
| | TCR γ/δ | Brilliant Violet 510™ | Armenian Hamster IgG | GL3 | BioLegend GmbH | 118131 | 50 |
| | CD62L | Brilliant Violet 605™ | Rat IgG2a, κ | MEL-14 | BioLegend GmbH | 104437 | 100 |
| | CD103 | Brilliant Violet 711™ | Armenian Hamster IgG | 2E7 | BioLegend GmbH | 121435 | 100 |
| | CD95 | APC | Rat IgG1, κ | SA367H8 | BioLegend GmbH | 152603 | 150 |
| | CD44 | PE | Rat IgG2b, κ | IM7 | BioLegend GmbH | 103023 | 150 |
| | KLRG1 | Brilliant Violet 421™ | Syrian Hamster IgG | 2F1/KLRG1 | BioLegend GmbH | 138413 | 100 |
| | CD183/CXCR3 | PE/ Cy7 | Armenian Hamster IgG | CXCR3-173 | BioLegend GmbH | 126515 | 100 |
| | CD69 | FITC | Armenian Hamster IgG | H1.2F3 | BioLegend GmbH | 104505 | 100 |
| | PD-1 | PE-Dazzle 594 | Rat IgG2b, κ | RMP1-30 | BioLegend GmbH | 109115 | 100 |
| Intracellular staining of T cells after stimulation | CD3 | APC/Cyanine7 | Rat IgG2b, κ | 17A2 | BioLegend GmbH | 100221 | 100 |
| | CD4 | FITC | Rat IgG2a, κ | RM4-5 | BioLegend GmbH | 100509 | 100 |
| | CD8a | Brilliant Violet 785™ | Rat IgG2a, κ | 53-6.7 | BioLegend GmbH | 100749 | 100 |
| | TCR γ/δ | Brilliant Violet 510™ | Armenian Hamster IgG | GL3 | BioLegend GmbH | 118131 | 50 |
| | T-bet | Brilliant Violet 711™ | Mouse IgG1, κ | 4B10 | BioLegend GmbH | 644819 | 100 |
| | GATA-3 | PE | Rat IgG2b, κ | IM7 | BioLegend GmbH | 653803 | 100 |
| | RORγT | PE-CF594 | Mouse IgG2a | Q31-378 | BD Biosciences | 562684 | 100 |
| | FoxP3 | PE-Cy5.5 | Rat / IgG2a, κ | FJK-16s | ThermoFisher Scientific | 35-5773-80 | 100 |
| | IFN-γ | Brilliant Violet 605™ | Rat IgG1, κ | XMG1.2 | BioLegend GmbH | 505839 | 150 |
| | IL-4 | Brilliant Violet 650™ | Rat IgG1 | 11B11 | BD Biosciences | 564004 | 100 |
| | IL-17A | Brilliant Violet 421™ | Rat IgG1, κ | TC11-18H10.1 | BioLegend GmbH | 506925 | 100 |
| | IL-10 | PE-Cy7 | Rat IgG2b, κ | JES516E3 | BioLegend GmbH | 505025 | 50 |
| | Granzyme B | Alexa Fluor® 647 | Mouse IgG1, κ | GB11 | BioLegend GmbH | 515405 | 100 |